

Part I

# Fundamentals of ES

COPYRIGHTED MATERIAL



# Chapter 1

---

## On the Mechanism of Electrospray Ionization Mass Spectrometry (ESIMS)

*Paul Kebarle\* and Udo H. Verkerk†*

*\*Department of Chemistry, University of Alberta, Edmonton, Alberta, Canada*

*†Center for Research in Mass Spectrometry, York University, Toronto, Ontario, Canada*

### 1.1 Introduction

#### 1.1.1 How It All Started

#### 1.1.2 Aims of This Chapter

#### 1.1.3 Electrospray, Other than Mass Spectrometric Applications

### 1.2 Production of Gas-Phase Ions by Electrospray and Electrospray Ionization Mass Spectrometry

#### 1.2.1 The Overall Process

#### 1.2.2 Production of Charged Droplets at the ES Capillary Tip. The Electrophoretic Mechanism

#### 1.2.3 Electrospray as an Electrolytic Cell of a Special Kind

#### 1.2.4 Required Electrical Potentials for ES. Electrical Gas Discharges

#### 1.2.5 Electrical Current, $I$ , due to the Charged Droplets. Charge and Radius of Droplets

#### 1.2.6 Solvent Evaporation from Charged Droplets Causes Droplet Shrinkage and Coulomb Fissions of Droplets

#### 1.2.7 Evolution of Droplets by Evaporation and Coulomb Fissions Producing Smaller and Smaller Progeny Droplets that Lead Ultimately to Minute Charged Droplets that Produce Ions in the Gas Phase

#### 1.2.8 Mechanisms for the Formation of Gas-Phase Ions from Very Small and Highly Charged Droplets: The Charged Residue Model (CRM) and the Ion Evaporation Model (IEM)

#### 1.2.9 The Iribarne–Thomson Equation for Ion Evaporation from Small Charged Droplets and Subsequent Experimental and Theoretical Work Examining the Validity of IEM

---

*Electrospray and MALDI Mass Spectrometry: Fundamentals, Instrumentation, Practicalities, and Biological Applications, Second Edition*, Edited by Richard B. Cole  
Copyright © 2010 John Wiley & Sons, Inc.

## 4 Chapter 1 On the Mechanism of Electrospray Ionization Mass Spectrometry (ESIMS)

- 1.2.10 Large Analyte Ions Such as Proteins and Dendrimers Are Most Probably Produced by the Charged Residue Model (CRM)
- 1.2.11 Dependence of the Observed Ion Abundance of Analytes on the Nature of the Analyte, on Its Concentration, and on the Presence of Other Electrolytes in the Solution
- 1.2.12 Noncovalent and Ionic Interactions in Solution and in the Gas Phase and other Relevant Differences Between Gas Phase and Solution
- 1.2.13 Some Examples of Effects on Mass Spectra of Proteins Due to the ESI Process
  - 1.2.13.1 Ion Pairing of Salt ions with Ionized Residues of Proteins
  - 1.2.13.2 Why Is Ammonium Acetate Such a Popular Salt Additive to Solutions Used for ESIMS
  - 1.2.13.3 Determinations by Electrospray of Equilibrium Constants of Association Reactions in Solution and Possible Sources of Error Due to the ESI Process
- 1.2.14 Nanoelectrospray and Insights into Fundamentals of Electrospray—Nanospray

References

## 1.1 INTRODUCTION

### 1.1.1 How It All Started

Electrospray ionization (ESI) is a method by which solutes present in a solution can be transferred into the gas phase as ions. The gas-phase ions can then be detected by mass spectrometric means (ESIMS). Remarkably, ESI can handle solutes such as polymers, nucleic acids, and proteins that have a very high molecular mass such as hundreds of megadaltons for proteins. The analytes present in the solution may be ions, such as the inorganic metal ions  $M^+$  and  $M^{2+}$  protonated amines or negative ions such as the halide ions  $X^-$  or deprotonated carboxylic acids, sulfates  $SO_4^{2-}$ , and so on. They can be also compounds that are neutral in the solution that is sprayed. In that case, the analyte is charged by association with one or more ions present in the solution. This charging process is part of the electrospray mechanism. ESIMS is the ideal method for detection of analytes from high-performance liquid chromatography or capillary electrophoresis. ESIMS is particularly valuable to biochemical, biomedical, and pharmacological research. The significance of ESIMS was recognized by a Nobel Prize in 2002 to John Fenn, who was the major developer of the method.<sup>1</sup>

ESIMS is actually the brainchild of Malcolm Dole. In the 1960s, Malcolm Dole was very interested in the determination of the molecular mass of synthetic polymers and developing a method with which one could observe such macromolecules by mass spectrometry. It was clear to him that mass spectrometric analysis of the polymer molecules could answer many questions and solve many problems. But how could one get large polymers into the gas phase without decomposing them? He had the idea that if one uses a very dilute solution of the analyte and then nebulized the solution into extremely small droplets, one might obtain many droplets that contained only one analyte molecule. Evaporation of the droplets would then lead to a transfer of the analyte molecules to the gas phase. If the analyte was not charged, as was often the case for synthetic polymers, the presence of an electrolyte, such as  $Na^+$  and  $Cl^-$  in the solution, could lead to charging of the polymer. Evaporation of a droplet that happens to contain one polymer molecule and one

$\text{Na}^+$  would lead to the desired charged analyte. However, for charging to occur, there has to be one or more functional groups on the analyte with which the ion can form a fairly strongly bonded complex in the absence of the solvent. For details of such complex formation see Section 1.2.13.1. In other droplets, there would be one  $\text{Cl}^-$  and one polymer, and that would lead to a negatively charged analyte that could be observed with the mass spectrometer in the negative ion mode. Such statistical charging was known to occur<sup>2</sup> and to be a rather inefficient source of ionized analytes.

Dole was preoccupied with thoughts on how to increase the efficiency, when a possible solution presented itself. While working as a consultant for a paint company,<sup>3</sup> he witnessed the electro spraying of paint on automobile bodies. The paint was sprayed on the cars very efficiently by very small charged paint droplets using a process known as electro spray. Applying electro spray to polystyrene solutions, Dole et al.<sup>4</sup> were able to develop an apparatus and demonstrate the production in the gas phase of polystyrene ions with molecular masses in the kilodalton range. While Dole's methods and results had some flaws and ambiguities, they clearly indicated that electro spray is a very promising soft ionization method for the mass spectrometry of macromolecules.

Dole et al.'s paper<sup>4</sup> caught the eye of Professor Seymour Lipsky at Yale Medical School. Lipsky, who was also involved with mass spectrometry, was very excited about the potential of electro spray for the mass spectrometric study of proteins. Dole et al.<sup>4</sup> had used a nozzle-skimmer system as the interface between the atmospheric pressure required for electro spray and the mass analysis region, and their paper contained a reference to work by John Fenn, who was a specialist in the field of molecular beams and their production by nozzle-skimmer systems. Through this reference, Lipsky got in touch with Fenn, who was also at Yale but at the Department of Mechanical Engineering. This contact inspired Fenn to start research on electro spray mass spectrometry. Since only a low-mass-range quadrupole was available in Fenn's laboratory, the first, pioneering papers<sup>5</sup> involved studies of small ions in the positive<sup>5a</sup> and negative ion<sup>5b</sup> mode. The ES ion source and interface to the mass analysis region were similar to those used by Dole, but included a few important changes such as the use of nitrogen gas counter flow at atmospheric pressure to remove solvent vapor caused by the droplet evaporation. This measure led to clean and relatively simple mass spectra that could be easily interpreted.

Subsequent work by Fenn and co-workers,<sup>6</sup> using a quadrupole mass analyzer with a high  $m/z$  range extending to  $m/z$  1500 and a heated capillary as the interface between the spray at atmospheric pressure and the vacuum containing the mass analysis section, clearly demonstrated that ESIMS could be used very effectively for analysis of peptides and proteins with molecular mass  $m$  which could be much higher than  $m = 1500$  daltons. This was possible because the use of ESI led to molecular ions that had multiple charges  $z$  so that the  $m/z$  value was lower than  $m/z = 1500$ . This work had a big impact and started the ESIMS revolution that is continuing to this day.

The development of ESIMS is clearly due to two people, Malcolm Dole and John Fenn. Dole's early death occurred before the full impact of ESIMS became evident. Fenn,<sup>1</sup> in his account on the development of the method, clearly acknowledges the seminal significance of Dole's work. Much of the information in this section is based on Fenn's account.<sup>1</sup>

### 1.1.2 Aims of This Chapter

This chapter is written for users of ESIMS. It presents an account of "how it all works." It addresses those just entering the field and more advanced users. Understanding of "how it all

works” is desirable not only from a standpoint of intellectual curiosity, but also for practical reasons. The mass spectra that one observes depend on a large number of parameters. These start with (a) a choice of solvent and concentrations of the analyte, (b) a choice of additives to the solution that may be beneficial, and (c) their concentration, choice of the flow rates of the solution through the spray capillary, the electrical potentials applied to the spray capillary (also called “needle”), and the potentials on the electrodes leading to the mass analysis. The choice of these parameters requires not only an understanding of conventional mass spectrometry but also an understanding of the electrospray mechanism as well as some familiarity with chemistry in solution as well as ion-molecule reactions in the gas phase. In early work on ESIMS, many of the parameters were established experimentally by trial and error; but now when a better understanding of the mechanism is at hand, it is certainly more efficient and analytically rewarding to understand the reasons for the choices.

Unfortunately, not all the processes that occur in ESIMS are well understood, and this has led to some controversy. However, enough is known to make the study of the mechanisms in ESIMS worthwhile.

The present chapter presents only a limited account of electrospray. A much more extensive coverage is provided by a review by Smith et al.<sup>7a</sup> While Smith’s review is quite old, most of the material is still very relevant.

### **1.1.3 Electrospray, Other than Mass Spectrometric Applications**

ES existed long before its application to mass spectrometry. It is a method of considerable importance for the electrostatic dispersion of liquids and creation of aerosols. The interesting history and notable research advances in that field are very well described in Bayley’s book<sup>7b</sup> *Electrostatic Spraying of Liquids*. Much of the theory concerning the mechanism of the charged droplet formation was developed by researchers in aerosol science. A compilation of articles in this area can be found in a special issue<sup>7c</sup> of the *Journal of Aerosol Science* devoted to electrospray.

## **1.2 PRODUCTION OF GAS-PHASE IONS BY ELECTROSPRAY AND ELECTROSPRAY IONIZATION MASS SPECTROMETRY**

### **1.2.1 The Overall Process**

There are three major steps in the production of gas-phase ions from electrolyte ions in solution. These are: (a) production of charged droplets at the ES capillary tip; (b) shrinkage of the charged droplets by solvent evaporation and repeated droplet disintegrations leading ultimately to very small highly charged droplets capable of producing gas-phase ions; and (c) the actual mechanism by which gas-phase ions are produced from the very small and highly charged droplets. Stages (a)–(c) occur in the atmospheric pressure region of the apparatus (see Figure 1.1).

Some of the ions resulting from the preceding stages (a)–(c) enter the vacuum region of the interface leading to the mass spectrometer either through a small orifice or through a sampling capillary (see Figure 1.2a,b). The ions may be clustered with solvent molecules and other additives and are subjected to (i) a thermal declustering “clean-up” in the heated capillary leading to the partial vacuum (pressure of a few torr) of the first chamber

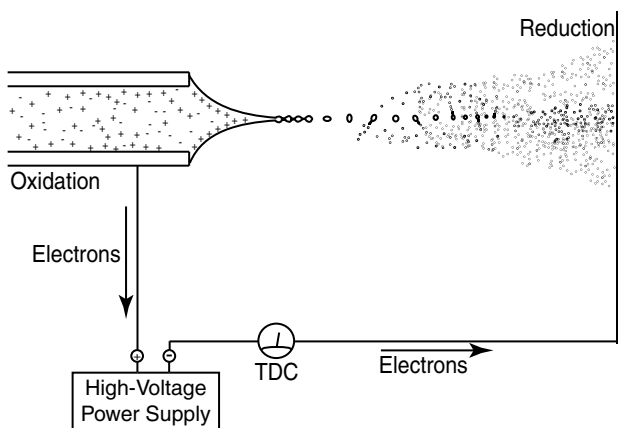


**Figure 1.1.** Schematic of major processes occurring in the atmospheric pressure region of electrospray. TDC stands for total droplet current ( $I$ ). This figure illustrates major processes occurring in the atmospheric pressure region of ESI run in the positive ion mode. Penetration of the imposed electric field into the liquid leads to formation of an electric double layer at the meniscus. The double layer is due to the polarizability and dipole moments of the solvent molecules and an enrichment near the meniscus of positive ions present in the solution. These cause a destabilization of the meniscus and formation of a cone and a jet charged by an excess of positive ions. The jet splits into droplets charged with an excess of positive ions. Evaporation of the charged droplets brings the charges closer together. The increasing Coulombic repulsion destabilizes the droplets that emit a jet of smaller charged progeny droplets. Evaporation of progeny droplets leads to destabilization and emission of second-generation progeny droplets, and so on, until free gas-phase ions form at some point.

and (ii) collisional activation due to an electric potential difference imposed between the sampling capillary exit and the skimmer leading to the second, high-vacuum chamber that is the housing of the mass spectrometer.

### 1.2.2 Production of Charged Droplets at the ES Capillary Tip. The Electrophoretic Mechanism

As shown in the schematic representation of the charged droplet formation (Figure 1.1), a voltage  $V_c$ , of 2–3 kV, is applied to the conductive capillary, which is typically 1 mm o.d. and located 1–3 cm from the counterelectrode. The counterelectrode in ESMS may be a plate with an orifice leading to the mass spectrometric sampling system or a sampling capillary, mounted on the plate, which leads to the MS (see Figure 1.2a). Because the spray capillary tip is very thin, the electric field  $E_c$  at the capillary tip is very high ( $E_c \approx 10^6$  V/m). The value of the field at the capillary tip opposite a large and planar counterelectrode can be evaluated with the approximate relationship<sup>8</sup>

$$E_c = 2V_c/[r_c \ln(4d/r_c)] \quad (1.1)$$

where  $V_c$  is the applied potential,  $r_c$  is the capillary outer radius, and  $d$  is the distance from capillary tip to the counterelectrode. For example, the combination  $V_c = 2000$  V,  $r_c = 5 \times 10^{-4}$  m, and  $d = 0.02$  m leads to  $E_c \approx 1.6 \times 10^6$  V/m. The field  $E_c$  is proportional to  $V_c$ , and the most important geometry parameter is  $r_c$ .  $E_c$  is essentially inversely proportional to  $r_c$ , while  $E_c$  decreases very slowly with the electrode separation  $d$ , due to the logarithmic dependence on  $d$ . For potentials required for electrospray, see Section 1.2.4.

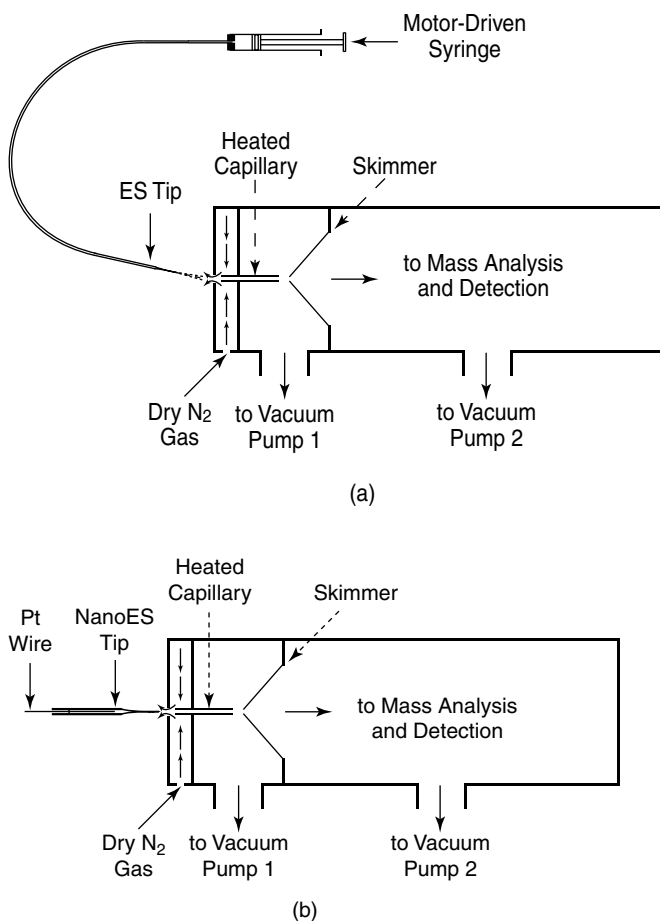


**Figure 1.2.** (a) Schematic of electro spray and interface to mass spectrometer. Solution containing analyte is supplied to the ES spray tip by a motor-driven syringe via flexible glass capillary tubing. A positive potential is applied to the spray tip (positive ion mode). The spray of positively charged droplets emerges from the spray capillary tip (see Figure 1.1). Solvent evaporation of the charged droplets leads to gas-phase ions. A mixture of ions, small charged droplets, and solvent vapor in the ambient gas enters the orifice leading to the nitrogen countercurrent chamber. The weak nitrogen countercurrent removes the solvent vapor; but the ions, driven by an electric potential and pressure difference, enter the heated capillary pathway into the low-pressure chamber. An electric field between this capillary and the skimmer cone accelerates the ions for a further collision activated "clean-up" of the ions. The potential difference over the cone orifice and downstream ion optical elements transports the ions into the high-vacuum region of the mass analysis chamber. (b) Same as Figure 1.2a but for nano electro spray. Large-diameter end of NanoES tip capillary is "loaded" with microliter amounts of solution. The electrical potential is supplied to the Nano tip either by a Pt wire or by a metal film coating the outside of the capillary. A spray of charged nano droplets results from the pull of the electric field on the polarized meniscus of the solution at the capillary tip.

A typical solution present in the capillary consists of a polar solvent in which the analyte is soluble. Because ESIMS is a very sensitive method, very low concentrations,  $10^{-7}$ – $10^{-3}$  moles/liter (M) of analyte need to be used. Methanol (or methanol–water) or acetonitrile (or acetonitrile–water) is often used as the solvent. For simplicity we will consider that the analyte is ionic and only the positive ion mode will be considered in the subsequent discussion.

When turned on, the field  $E_c$  will penetrate the solution near the capillary tip. This will cause a polarization of the solvent near the meniscus of the liquid. Assuming that the solvent is water, the field will align the permanent dipoles of  $H_2O$  so that on the average there will be many molecules oriented with the H atoms pointing downfield. Due to the polarizability of the  $H_2O$  molecule, induced dipoles with the same downfield orientation will also result. In the presence of even traces of an electrolyte, the solution will be sufficiently conducting and the positive and negative electrolyte ions in the solution will move under the influence of the field. This will lead to an enrichment of positive ions near the surface of the meniscus and negative ions away from the meniscus. The combined downfield forces due to these processes cause a distortion of the meniscus into a cone pointing downfield (see Figure 1.1). The increase of surface due to the cone formation is resisted by the surface tension of the liquid. The cone formed is called a Taylor cone (see Taylor<sup>9</sup> and Fernandez de la Mora<sup>10</sup>). If the applied field is sufficiently high, a fine jet emerges from the cone tip, whose surface is charged by an excess of positive ions. The jet breaks up into small charged droplets (see Figure 1.1; for a more accurate representation of the cone jet mode, see Figure 1.3a, due to Cloupeau<sup>11a</sup>).

It is apparent from Figure 1.3a that the size of the droplets formed from the cone jet is dependent on the jet diameter  $2R_j$ , and therefore all droplets produced could be expected to be approximately of the same size—that is, approximately monodisperse. This was proposed by Cloupeau<sup>11a</sup> and confirmed by studies of Tang and Gomez.<sup>12</sup> Also shown in Figure 1.3a is a much smaller “satellite” droplet. The satellite droplets are commonly observed, but their role in the ultimate formation of gas-phase ions out of the charged droplets is probably minor.

The droplets are positively charged due to an excess of positive electrolyte ions at the surface of the cone and the cone jet. Thus, if the major electrolyte present in the solution was ammonium acetate, the excess positive ions at the surface will be  $NH_4^+$  ions. This mode of charging, which depends on the positive and negative ions drifting in opposite directions under the influence of the electric field, has been called the electrophoretic mechanism.<sup>11b,c</sup> The charged droplets produced by the cone jet drift downfield through the air toward the opposing electrode. Solvent evaporation at constant charge leads to droplet shrinkage and an increase of the electric field normal to the surface of the droplets. At a given radius, the increasing repulsion between the charges overcomes the surface tension at the droplet surface. This causes a coulomb fission of the droplet, also called a coulomb explosion. The droplet fission occurs, via formation of a cone and a cone jet that splits into a number of small progeny droplets. This process bears close resemblance to the cone jet formation at the capillary tip (see Fernandez de la Mora<sup>10</sup> and references therein). Further evaporation of the

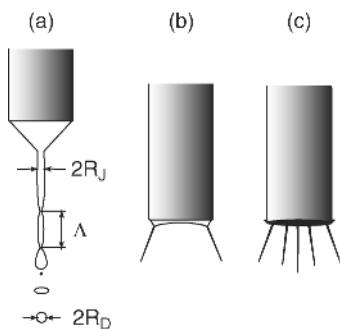


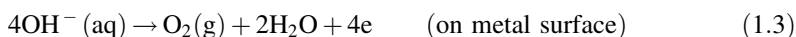
**Figure 1.3.** Different forms of electrospray at the tip of the spray capillary. (a) Cone jet mode. Relationship between radius of droplets and radius of jet:  $R_D/R_j \approx 1.9$ . Much smaller, satellite droplets can also be produced (see small droplet in this figure). These are more common at higher flow rates. In such cases, two types of monodisperse droplets are observed: the large progeny droplets and the small (satellite) progeny. (b), (c) Multijet modes result as the spray voltage is increased and the flow rate imposed by the syringe is high. (After Cloupeau.<sup>11a</sup>)

parent droplet leads to repeated fissions. The progeny droplets also evaporate and fission. More details on these processes are given in Section 1.2.6. Very small charged droplets result that lead ultimately to gas-phase ions by processes that will be described in detail in subsequent sections.

The cone-jet mode at the spray capillary tip described and illustrated in Figure 1.1 and Figure 1.3a is only one of the possible ES modes. For a qualitative description of this and other modes, see Cloupeau<sup>11a-c</sup>. More recent studies by Vertes and co-workers<sup>11d</sup> using fast time-lapse imaging of the Taylor cone provide details on the evolution of the Taylor cone into a cone jet and pulsations of jet. The pulsations lead to spray current oscillations. The current oscillations are easy to determine with conventional equipment and can be used as a guide for finding conditions that stabilize the jet and improve signal-to-noise ratios of the mass spectra. The cone-jet mode is most often used in ESIMS. It is also the best-characterized mode in the electrospray literature<sup>7,10-12</sup> and references therein.

### 1.2.3 Electrospray as an Electrolytic Cell of a Special Kind

At a steady operation of the electrospray in the positive ion mode (see Figure 1.1), the positive droplet emission will continuously carry off positive charge. The requirement for charge balance in such a continuous electric current device, together with the fact that only electrons can flow through the metal wire supplying the electric potential to the electrodes (Figure 1.1), leads to the supposition that the ES process must include an electrochemical conversion of ions to electrons. In other words, the ES device can be viewed as a special type of electrolytic cell.<sup>13</sup> It is special because the ion transport does not occur through uninterrupted solution, as is normally the case in electrolysis. In the positive ion mode, part of the ion transport occurs through the gas phase where positively charged droplets and later positive gas-phase ions are the charge carriers. A conventional electrochemical oxidation reaction should be occurring at the positive electrode—that is, at the liquid–metal interface of the capillary (Figure 1.1). This reaction should be supplying positive ions to the solution. The nature of these ions depends on the experimental conditions. If the spray capillary is made out of metal, the neutral metal ions can become oxidized to the positive ionic state by releasing electrons to the metal electrode and entering the solution [see Eq. 1.2]. The other alternative is the removal of negative ions present in the solution by an oxidation reaction as illustrated below [Eq. 1.3] for aqueous solutions:



One expects that the reaction with the lowest oxidation potential will dominate, and that reaction will depend on the material present in the metal electrode, the ions present in the solution, and the nature of the solvent. Proof for the occurrence of an electrochemical oxidation at the metal capillary was provided by Blades et al.<sup>13</sup> When a Zn capillary tip was used, release of  $\text{Zn}^{2+}$  to the solution could be detected. Furthermore, the amount of  $\text{Zn}^{2+}$  release to the solution per unit time when converted to coulombs/second was found to be equal to the measured electrospray current,  $I$  (Figure 1.1). Similar results were observed with stainless steel capillaries.<sup>13</sup> These were found to release  $\text{Fe}^{2+}$  to the solution. These quantitative results provided the strongest evidence for the electrolysis mechanism.

It should be noted that the oxidation reaction described in Eq. 1.2 adds ions that were not present previously in the solution. On the other hand, the oxidation, Eq. 1.3, provides the

positive current by removing the negative counterions of positive ions that are already present in the solution. The excess unipolar ions provided to the solution when expressed as concentrations in the solution amount to very low concentrations. Taking the Zn capillary tip as example, a solution of  $10^{-5}$  M NaCl in methanol at a flow rate  $V_f = 20 \mu\text{L}/\text{min}$  was found to lead to an electrospray current of  $1.6 \times 10^{-7}$  A. The  $\text{Zn}^{2+}$  concentration produced by the Zn-tipped capillary evaluated from the current was  $[\text{Zn}^{2+}] = 2.2 \times 10^{-6}$  M. Assuming that the  $\text{Na}^+$  ion was the analyte ion, the concentration of the ions produced by the oxidation at the electrode is only  $\sim 1/5$  of that of the analyte. It will be shown later that the electrospray current,  $I$ , increases very slowly with the total electrolyte concentration. Therefore, at higher total electrolyte concentrations due to analyte and additives, the ions produced by oxidation at the electrode may not be noticed in the mass spectrum because of the nature of the charges on the droplets that will ultimately lead to the detected ions. That is, one must consider all of the positive ions in solution and not only the positive ions produced at the positive electrode.

Van Berkel and co-workers, in a series of publications, have examined the consequences of the electrochemical processes to ESIMS. For a summary, see Chapter 3 by Van Berkel in this book. For example, they were able to demonstrate<sup>14</sup> that ions produced by the electrolysis process, such as hydrogen ions, can in some cases have important effects on the mass spectra obtained with pH-sensitive analytes such as nondenatured proteins.

Surprisingly, some skepticism on the significance to ESIMS of the electrochemically produced ions has been expressed in the literature and this led to a special issue of the *Journal of Mass Spectrometry*.<sup>15</sup> The consensus derived from this special issue is that for the typical ESIMS apparatus that provides a continuous unipolar charged droplet current, see Figure 1.1, an electrochemical process does occur at the spray electrode, in agreement with Blades et al.<sup>13</sup> and the work of van Berkel and coworkers. Most often, the ions created by the electrolytic process do not interfere with the analytical MS work. However, there are cases when one needs to consider the effect of the electrolytic ions.

### 1.2.4 Required Electrical Potentials for ES. Electrical Gas Discharges

D. P. H. Smith<sup>16</sup> was able to derive a very useful approximate equation for the required electric field,  $E_{\text{on}}$ , at the capillary tip, which leads to an onset of instability of a static Taylor cone and to the formation of a jet at the apex of the cone.

$$E_{\text{on}} \approx \left( \frac{2\gamma \cos \theta}{\epsilon_0 r_c} \right)^{1/2} \quad (1.4)$$

This equation for the onset field, when combined with Eq. 1.1, leads to an equation for the potential,  $V_{\text{on}}$ , required for the onset of electrospray:

$$V_{\text{on}} \approx \left( \frac{r_c \gamma \cos \theta}{2\epsilon_0} \right)^{1/2} \ln(4d/r_c) \quad (1.5)$$

where  $\gamma$  is the surface tension of the solvent,  $\epsilon_0$  is the permittivity of vacuum,  $r_c$  is the radius of the capillary, and  $\theta$  is the half-angle for the Taylor cone. Substituting the values  $\epsilon_0 = 8.8 \times 10^{-12} \text{ J}^{-1} \text{ C}^2$  and  $\theta = 49.3$  (see Taylor<sup>9</sup>), one obtains

$$V_{\text{on}} = 2 \times 10^5 (\gamma r_c)^{1/2} \ln(4d/r_c) \quad (1.6)$$

**Table 1.1.** Onset Voltages,  $V_{\text{on}}$ , for Solvents with Different Surface Tension,  $\gamma$ 

Solvent	CH <sub>3</sub> OH	CH <sub>3</sub> CN	(CH <sub>3</sub> ) <sub>2</sub> SO	H <sub>2</sub> O
$\gamma$ (N/m)	0.0226	0.030	0.043	0.073
$V_{\text{on}}$ (kV)	2.2	2.5	3.0	4.0

where  $\gamma$  must be substituted in Newtons per meter and  $r_c$  in meters to obtain  $V_{\text{on}}$  in volts. Shown in Table 1.1 are the surface tension values for four solvents and the calculated electrospray onset potentials for  $r_c = 0.1$  mm and  $d = 40$  mm. The surface of the solvent with the highest surface tension (H<sub>2</sub>O) is the most difficult to stretch into a cone and jet, and this leads to the highest value for the onset potential  $V_{\text{on}}$ .

Experimental verification of Eqs. (1.5)–(1.7) has been provided by Smith,<sup>16</sup> Ikonomou et al.,<sup>17</sup> and Wampler et al.<sup>18</sup> For stable ES operation, one needs to go a few hundred volts higher than  $V_{\text{on}}$ . Use of water as the solvent can lead to the initiation of an electric discharge from the spray capillary tip, particularly when the capillary is negative—that is, in the negative ion mode. The electrospray onset potential  $V_{\text{on}}$  is the same for both the positive and negative ion modes; however, the electric discharge onset is lower when the capillary electrode is negative<sup>17,18</sup> and metallic. This is probably due to emission of electrons from the negative capillary which initiate the discharge. Use of capillaries that are made out of glass where the electrical potential is applied via an internal metal wire that is embedded in the solution reduces the risk of electric discharge. For an illustration see Figure 1.2b. Neat water as solvent can be used with this arrangement and nanoelectrospray in the positive ion mode without the occurrence of electric discharge.

The occurrence of an electric discharge leads to an increase of the capillary current,  $I$ . Currents above  $10^{-6}$  A are generally due to the presence of an electric discharge. A much more specific test is provided by the appearance of discharge-characteristic ions in the mass spectrum. Thus, in the positive ion mode the appearance of protonated solvent clusters such as H<sub>3</sub>O<sup>+</sup>(H<sub>2</sub>O)<sub>*n*</sub> from water or CH<sub>3</sub>OH<sub>2</sub><sup>+</sup>(CH<sub>3</sub>OH)<sub>*n*</sub> from methanol indicates the presence of a discharge.<sup>17</sup> The protonated solvent ions are produced at high abundance by ES in the absence of a discharge, only when the solvent has been acidified—that is, when H<sub>3</sub>O<sup>+</sup> and CH<sub>3</sub>OH<sub>2</sub><sup>+</sup> are present in the solution.

The presence of an electric discharge degrades the performance of ESMS, particularly so at high discharge currents. The electrospray ions are observed at much lower intensities than was the case prior to the discharge, and the discharge-generated ions appear with very high intensities.<sup>17,18</sup>

The high potentials required for electrospray show that air at atmospheric pressure is not only a convenient, but also a very suitable, ambient gas for ES, particularly when solvents with high surface tension, such as water, are to be electrosprayed. The oxygen molecules in air have a positive electron affinity and readily capture free electrons. Initiation of gas discharges occurs when free electrons present in the gas (due to cosmic ray or background radiation) are accelerated by the high electric field near the capillary to velocities where they can ionize the gas molecules. At near-atmospheric pressures, the collision frequency of the electrons with the gas molecules is very high and interferes with the electron acceleration process.

The presence of gases that capture electrons and convert them to atomic or molecular negative ions suppress the electrical breakdown. SF<sub>6</sub> and polychlorinated hydrocarbons also capture electrons and are more efficient discharge-suppressing gases than O<sub>2</sub>. SF<sub>6</sub> has

been used to advantage for the suppression of discharges in electrospray.<sup>16–18</sup> Use of these trace gas additives prevents gas discharges even when neat water is used as solvent.<sup>17,18</sup>

### 1.2.5 Electrical Current, $I$ , due to the Charged Droplets. Charge and Radius of Droplets

The electrical current,  $I$ , due to the charged droplets leaving the ES capillary is easily measured (see Figure 1.1) and of interest because it provides a quantitative measure of the total number of the excess positive ionic charges that leave the capillary and could be converted to gas-phase ions.

Fernandez de la Mora and Locertales<sup>19</sup> have proposed the following approximate relationships, on the basis of experimental measurements of the current,  $I$ , and droplet sizes and charges, together with theoretical reasoning:

$$I = f\left(\frac{\varepsilon}{\varepsilon_0}\right)\left(\gamma KV_f \frac{\varepsilon}{\varepsilon_0}\right)^{1/2} \quad (1.7)$$

$$R \approx (V_f \varepsilon / K)^{1/3} \quad (1.8)$$

$$q \approx 0.7[8\pi(\varepsilon_0 \gamma R^3)^{1/2}] \quad (1.9)$$

where  $\gamma$  is surface tension of solvent,  $\varepsilon$  is permittivity of solvent,  $\varepsilon_0$  is permittivity of vacuum (free space),  $\varepsilon/\varepsilon_0$  is dielectric constant of solvent,  $K$  is conductivity of solution,  $E$  is applied electric field at capillary tip [see (Eq. 1.2)],  $R$  is radius of droplets produced at capillary tip,  $q$  is charge of droplets, and  $V_f$  is flow rate, volume/time.  $f(\varepsilon/\varepsilon_0)$  is a numerical function tabulated by the authors<sup>19</sup>; the value of  $f(\varepsilon/\varepsilon_0)$  is approximately 18 for liquids whose dielectric constant,  $\varepsilon/\varepsilon_0$ , is  $\geq 40$ . This includes water ( $\varepsilon/\varepsilon_0 = 78$ ) and water–methanol mixtures as well as acetonitrile and formamide. The relationships were obtained for solutions having conductivities  $K$  larger than  $10^{-4} \text{ S m}^{-1}$ . For polar solvents like water and methanol, as well as for electrolytes that dissociate essentially completely to ions, this requirement corresponds to solutions with concentrations higher than  $\sim 10^{-5} \text{ mol/L}$ —that is, a concentration range that is commonly present in ESMS. The flow rates used<sup>19</sup> were below  $1 \mu\text{L/min}$  and are thus close to the flow rates used in conventional ESIMS. The equation is valid when the spray is operated in the cone jet mode.

More recently, a theoretical treatment by Cherney<sup>20</sup> has confirmed the deductions of Fernandez de la Mora and Locertales and provided a more detailed description of the conditions existing in the conejet. The treatment is also in agreement with recent experimental data by Chen and Pui.<sup>21</sup>

### 1.2.6 Solvent Evaporation from Charged Droplets Causes Droplet Shrinkage and Coulomb Fissions of Droplets

The charged droplets produced by the spray needle shrink due to solvent evaporation while the charge remains constant. The energy required for the evaporation is provided by the thermal energy of the ambient air. As the droplet gets smaller, the repulsion of the charges at the surface increases and at a certain droplet radius the repulsion of the charges overcomes the cohesive force of the surface tension. A Coulomb instability results and leads

to a fission of the droplet that typically releases a jet of small charged progeny droplets. The condition for the Coulomb instability is given by the Rayleigh<sup>22</sup> equation:

$$Q_{\text{Ry}} = 8\pi(\epsilon_0\gamma R^3)^{1/2} \quad (1.10)$$

where  $Q_{\text{Ry}}$  is the charge on the droplet,  $\gamma$  is the surface tension of the solvent,  $R$  is the radius of the droplet and  $\epsilon_0$  is the electrical permittivity. The shrinkage of the droplets at constant charge and the fission at or near the Rayleigh limit with the release of a jet of small, close to monodisperse, charged progeny droplets has been confirmed by a number of experiments. A single droplet from the spray was introduced at ambient pressure into an apparatus that allowed determination of the diameter and the charge of the droplet and the droplet observed until jet fission occurred.<sup>23–28</sup> Most studies have used some form of electrodynamic balance (EDB) that confines the charged droplet to a small region of space where it can be observed by optical methods. The EDB method is not well-suited for rapidly evaporating solvents such as methanol or water. Therefore, EDB has been applied mainly to relatively nonvolatile solvents. Davis et al.<sup>23</sup> were able to study water using a quadrupole ion trap but with the use of a surfactant that slowed down the evaporation.

A second method used by Gomez and Tang<sup>24</sup> is better suited for volatile solvents. It relies on phase Doppler interferometry (PDI). This method allows *in situ* measurements of the size and velocity of the electrosprayed droplets but not the charge, which must be inferred from other data. More recently, PDI was used by Beauchamp and co-workers,<sup>25</sup> who obtained the charge of the droplets from a comparison of the measured and calculated droplet mobilities. A concise summary of results by these and other authors (Taflin et al.,<sup>26</sup> Richardson et al.,<sup>27</sup> and Schweizer et al.<sup>28a</sup>) is given in Table 1.2. One can deduce from the

**Table 1.2.** Experimental Observations of Charged Droplets and Their Breakup

Authors	Solvent	Droplet diameter range ( $\mu\text{m}$ )	Onset of Instability (%) of Rayleigh limit	% of Mass Lost in Breakup	% of Charge Lost in Breakup
Beauchamp and co-workers <sup>25a</sup>	Water	10–40	90	N.D. <sup>a</sup>	20–40
	Methanol	10–40	110	N.D.	15–20
	Acetonitrile	10–40	100	N.D.	15–20
Grimm and Beauchamp <sup>25b</sup>	<i>n</i> -Heptane	35–45	100	N.D.	19
	<i>n</i> -Octane		87	N.D.	17
	<i>p</i> -Xylene		89	N.D.	17
Davis and Bridges <sup>23</sup>	Water with surfactant	4–20	90	1–2	15–25
Gomez and Tang <sup>24</sup>	Heptane	20–100	70	N.D.	N.D.
	Low-vapor-pressure oils	4–20	75–85	2	10–15
Richardson et al. <sup>27</sup>	Diocetyl Phthalate	Not reported	102–84	2.3	15–50
Schweizer and Hanson <sup>28a</sup>	<i>n</i> -Octanol	15–40	96–104	5	23
	Ethylene glycol	20–30	100	0.3	33

<sup>a</sup> N.D., not determined.

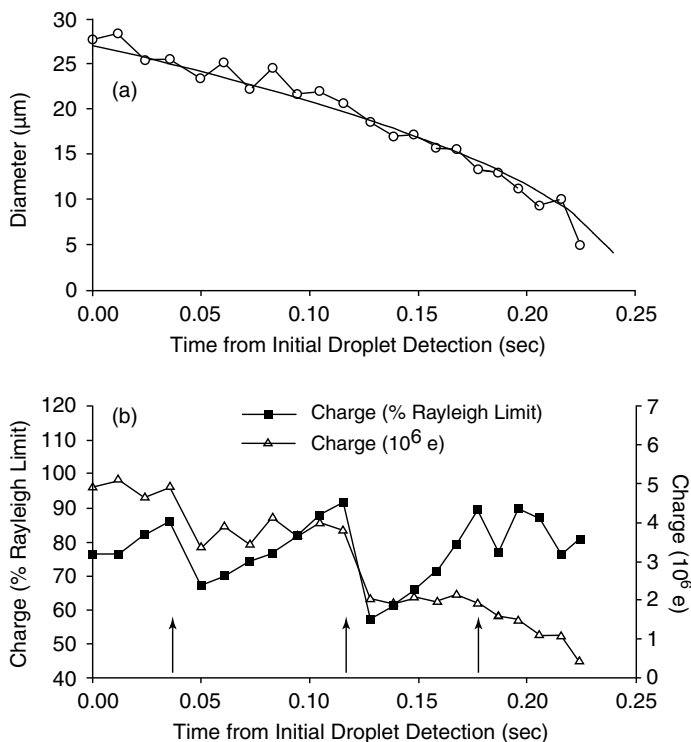


**Figure 1.4.** Evaporation and discharge of a positively charged water droplet in nitrogen gas at ambient pressure and 317 K and a weak (51 V/cm) electric field. (a) Variation of droplet diameter with time. Also plotted (smooth curve) is the predicted change of diameter due to evaporation of a neutral water droplet in a vapor-free  $\text{N}_2$  gas at 317 K. (b) Variation of droplet charge with time, represented as number of elementary charges and as percent of the Rayleigh limit. Arrows indicate discharge events. Note that water droplets undergo a Coulomb fission at approximately 90% of the Rayleigh limit and are at approximately 65% of the limit after the Coulomb fission. (Figure from Grimm and Beauchamp,<sup>30a</sup> with permission from the American Chemical Society.)

table that the dependence on the type of solvent is relatively small. Thus, droplets from all solvents experience Coulomb fissions close to, or at, the Rayleigh limit. The loss of mass on fission is between 2% and 5% of the parent droplet, and the loss of charge is much larger—that is, some 15–25% of the charge of the parent droplet.

Beauchamp and co-workers<sup>25</sup> also provide information on the charge of the parent droplet immediately after the droplet fission. An example of such data is given in Figure 1.4, where the charge of the droplets before and after the fission is given as percent of the Rayleigh condition [Eq. 1.10]. These, along with results for the other solvents studied,<sup>25</sup> show that the evaporating charged droplets oscillate at all times between fairly narrow limits of the Rayleigh condition. This finding has bearing on the discussion of the mechanism by which non-denatured proteins enter the gas phase (see charged residue mechanism in Section 1.2.10). Notable also (see Figure 1.4a) is the observation that the diameter of the charged parent droplet undergoing evaporation *and* Coulomb fissions remains very close to the diameter of an uncharged droplet that loses mass only due to evaporation. [For equations used to evaluate the change of diameter of the uncharged

droplet with time due to evaporation only, see Eq. (1.2)–(1.4) in Grimm and Beauchamp.<sup>25b</sup>] This result supports the observations of Davis and Bridges,<sup>23</sup> Taflin et al.,<sup>26</sup> and Richardson et al.<sup>27</sup> (see Table 1.2) that the total mass that goes into the charged progeny droplets is very small. Duft et al.,<sup>28b</sup> using ethylene glycol droplets with a radius of 25  $\mu\text{m}$  and an arrangement that allowed high-speed microscopic images of the droplets to be obtained, report that 33% of the charge and only 0.3% of the mass goes into about 100 progeny droplets and that the progeny droplets, when formed, are below but very close to the Rayleigh limit.

When the sprayed solution contains a solute, such as a salt, the continuous evaporation of the droplets will lead to very high concentrations of the salt and finally to charged solid particles—the “skeletons” of the charged droplets. These skeletons can reveal some aspects of the droplet evolution. Fernandez de la Mora and co-workers<sup>29</sup> have used this approach to study charged droplet evolution. This work is of special relevance to the ion evaporation model and is discussed in Section 1.2.9.

Fission of charged droplets can be forced to occur also below the Rayleigh limit when the charged droplet is exposed to a strong electric field. In this case, the excess charges on the droplet are forced to move downfield and accumulate on the downfield side. The force exerted by this asymmetric charge distribution overcomes the surface tension of the droplet and causes a downfield distortion of the droplet and the formation of a cone and cone-jet that splits into charged progeny droplets. This field-induced droplet ionization (FIDI) has been studied in some detail by Grimm and Beauchamp,<sup>30</sup> who created the droplets with a vibrating orifice aerosol generator (VOAG). An example of this work is shown in Figure 1.5, which documents the gradual distortion with time of the droplet and the ultimate formation of the cone-jet and progeny droplets. Notable are the low charges of the droplet that still can lead to droplet fission when a high enough field is present. Thus a droplet with only 4% of the Rayleigh charge can be forced to emit a cone-jet by a field,  $E = 2.15 \times 10^6$  V/m (see Figure 1.5).

This field is not far from the field needed to start conventional ES, with a spray capillary [see Eq. 1.1 in Section 1.2.2]. This indicates that near the spray capillary, Coulomb fissions of the charged droplets could be occurring before droplet evaporation has brought the droplet diameter down to the Rayleigh limit.

Grimm and Beauchamp<sup>30b</sup> have shown that the gas-phase ions ultimately resulting from FIDI can be detected with a mass spectrometer and that the method might have some analytical potential. These experiments bear some resemblance to earlier work by Hager et al.,<sup>31</sup> who also produced neutral droplets with a vibrating orifice and then exposed them to a nonhomogeneous electric field near a rod electrode and detected the ions with a mass spectrometer. These authors named the method “droplet electrospray.” As could be expected, due to the small number of droplets, the sensitivity of the droplet method<sup>31</sup> was much lower than that obtained with ESIMS.

A variation of the FIDI method demonstrated by Grim and Beauchamp<sup>30a</sup> could have significant analytical utility. In this case, neutral droplets containing an electrolyte were exposed to a homogeneous high electric field. The field forced the negative ions in the solution to one side of the field and forced the positive to the other side. The induced instability of the droplet leads ultimately to a symmetric fission of the droplet, and negatively and positively charged jets of progeny droplets are emitted on the opposite sides. This experiment should allow the mass spectrometric observation of the positive and negative ions in the solution, which in certain cases could be of special analytical interest.

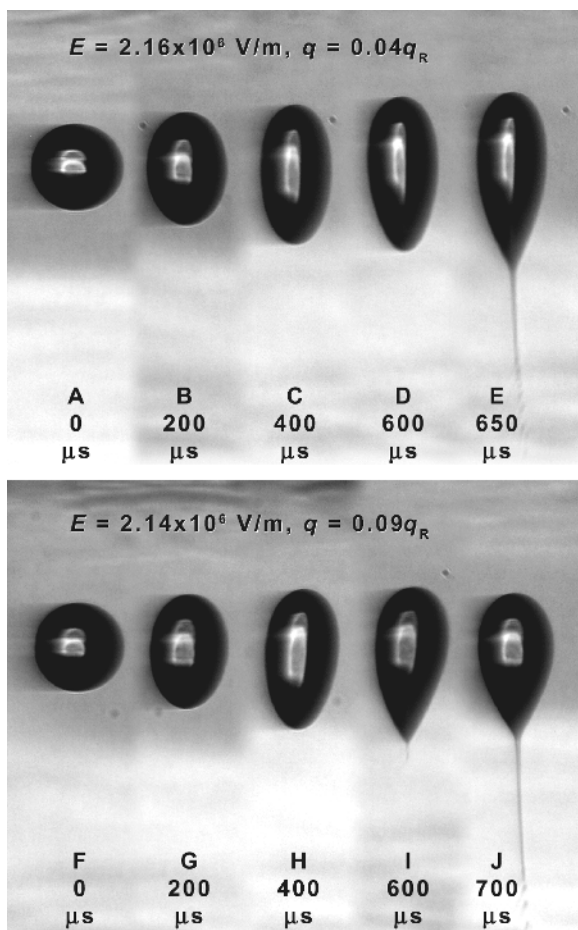


**Figure 1.5.** Sequences of 225- $\mu\text{m}$ -diameter methanol droplets with a charge of  $q = 0.04q_R$ , where  $q_R$  is the charge when the droplet is at the Rayleigh limit. Droplets undergoing asymmetrical distortions at an applied electric field,  $E = 2.16 \times 10^6 \text{ V/m}$  and in the second row droplets with  $q = 0.09q_R$  and  $E = 2.14 \times 10^6 \text{ V/m}$ . In both cases these fields represent the minimum for which field-induced droplet ionization (FIDI) is observed. The jets in frames E and J demonstrate capillary instability and the formation of progeny droplets of approximately 10- $\mu\text{m}$  diameter. For the  $q = 0.04q_R$ , the time of 650  $\mu\text{s}$  for jetting to begin is identical to that observed for a neutral droplet. (From Grimm and Beauchamp,<sup>30b</sup> with permission from the American Chemical Society.)

### 1.2.7 Evolution of Droplets by Evaporation and Coulomb Fissions Producing Smaller and Smaller Progeny Droplets that Lead Ultimately to Minute Charged Droplets that Produce Ions in the Gas Phase

It is clear that the process of repeated droplet fissions of parent droplets that lead to smaller parent droplets and progeny droplets, along with the evaporation of the progeny droplets that lead to second generation progeny, will ultimately lead to very small charged droplets that are the precursors of the gas-phase ions. The mechanisms by which the gas phase ions are produced from the very small “final” droplets is considered in Section 1.2.8. Here we examine some of the details of the evolution of the initial droplets, formed at the spray capillary, to droplets that are the precursors of the ions. The whole process is driven by the decrease of droplet volume by evaporation. The continuous evaporation is possible because the thermal energy required for the evaporation is provided by the ambient gas, air or pure nitrogen, at near atmospheric pressure. As will be shown below, a very large loss of solvent by evaporation occurs before the very small droplets that lead to ions are formed.

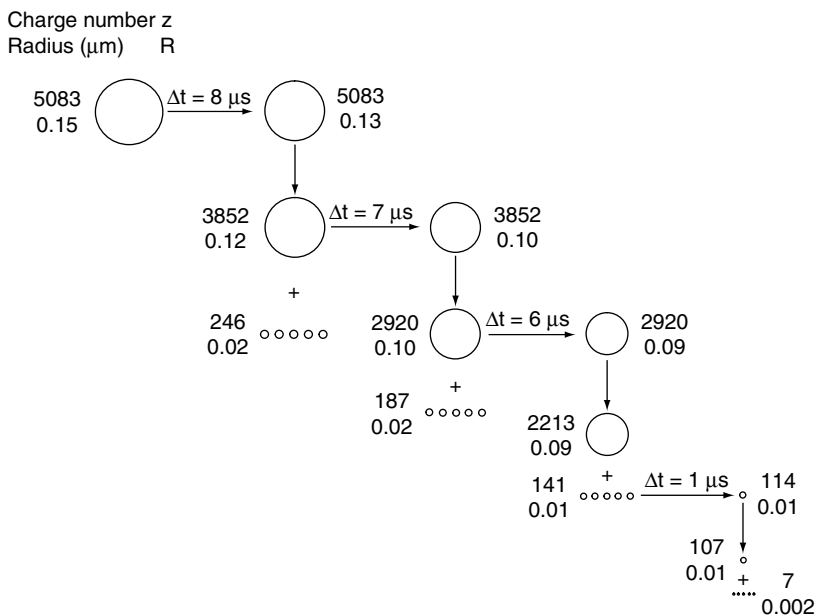


**Figure 1.6.** Droplet history of charged water droplets produced by nanospray. The first droplet is one of the droplets produced at spray needle. This parent droplet is followed for three evaporation and fission events. The first-generation progeny droplets are shown, along with the fission of one of the progeny droplets that leads to second-generation progeny droplets.  $R$  is the radius of the droplets and  $Z$  gives the number of charges on the droplet.  $Z$  corresponds to the number of excess singly charged ions near the surface of the droplet. The parents charge is  $Z = 0.9Z_R$  just before the fission and  $Z = 0.7Z_R$  just after the fission (as observed in Figure 1.4), while the progeny droplets have  $Z = 0.7Z_R$  just after the fission of the parent. (Based on Figure 1.1 in Peschke, Verkerk, and Kebarle.<sup>32</sup>)

It is desirable to be able to estimate the increase of solute concentration due to the volume loss, particularly so in certain applications of ESIMS. An example is the determination of association constants of protein–ligand complexes by the titration method (see Section 1.2.13.3).

A droplet evolution scheme is shown in Figure 1.6. It deals with droplets produced by nanoelectrospray. The nanospray droplets are better suited for the evaluation of droplet histories because the evolution is much shorter. The very much smaller initial droplets reach much faster the final stage of very small charged droplets that lead to ions.

The assumptions with which the scheme (Figure 1.6) for water as solvent was obtained are described in detail in the section entitled “Calculations and Experimental” in Peschke et al.<sup>32</sup> The stability limits of droplet fission at droplet charge  $Z = 0.9Z_R$  (just before the droplet fission) and  $Z = 0.7Z_R$  (just after the fission due to Beauchamp and co-workers<sup>25a</sup> for water) were used (see Figure 1.4 in the present work). These are for droplets of radii in the 13- to 3- $\mu\text{m}$  range, while the nano-droplet evolution scheme (Figure 1.6) involves close to a hundred times smaller radii. It is not known to what extent the droplet fissions of such small droplets follow the same stability limits. Unfortunately, no measurements for such small droplets exist because these droplets evaporate and fission very fast, within several microseconds, while the large droplets<sup>30a</sup> fission within intervals of some 40 ms (see Figure 1.4).

Using the droplet radii, one can evaluate that approximately 40% of the volume is lost between each fission. A corresponding increase by 40% of the solute concentration must also occur. This means that after 10 successive fissions of the parent droplet, its volume will decrease 29-fold and the concentration of solutes in the droplet will also increase 29-fold.

### 1.2.8 Mechanisms for the Formation of Gas-Phase Ions from Very Small and Highly Charged Droplets: The Charged Residue Model (CRM) and the Ion Evaporation Model (IEM)

Two mechanisms have been proposed to account for the formation of gas-phase ions from very small and highly charged droplets. The first mechanism, proposed by Dole et al.,<sup>4</sup> depends on the formation of extremely small droplets that could contain one analyte molecule and some ionic charges. Solvent evaporation from such a droplet will lead to a gas-phase analyte ion whose charge originates from the charges at the surface of the vanished droplet. This assumption is now known as the *charged residue model* (CRM). Early support for the mechanism was provided by Rollgen and co-workers.<sup>33</sup>

Iribarne and Thomson<sup>34</sup> proposed a different mechanism for the production of gas-phase ions from the charged droplets. The Iribarne *Ion Evaporation Model* (IEM) is described in some detail in the next section. It predicts that, after the radii of the droplets decrease to a given size, direct ion emission from the droplets becomes possible. This process, which they called *ion evaporation*, becomes dominant over Coulomb fission for droplets with radii of  $R \leq 10$  nm (*vide infra*).

Iribarne and Thomson<sup>34</sup> did not use electrospray to produce the small droplets. They were interested in the nature of the charged species produced from very small droplets obtained from pneumatic “atomization” of a liquid such as water containing a solute such as NaCl. Some of the droplets will be charged due to statistical imbalances between positive and negative electrolyte ions present in the droplets. The charged droplets of different polarities were separated by the application of a weak electric field. The charged droplets evaporate rapidly and lead to charged salt particles—that is, charged salt clusters. Iribarne and Thomson obtained ion mobility spectra of the charged particles and observed an isolated high-intensity peak at the high mobility end of the spectrum and a very broad and dense region of peaks at low mobilities. Changing the concentration of the salt did not change the position of the high-mobility peak. These results suggested that the high-mobility peak is due to single ions such as  $\text{Na}^+$  while multiply charged, larger salt aggregates were producing the broad and dense region of peaks at low mobilities. Much earlier (1937), on the basis of extensive mobility studies of such charged species, Chapman,<sup>2a</sup> also using “atomization,” had come to the same conclusion. In later work by Thomson and Iribarne,<sup>34b</sup> the ions were sampled with a mass spectrometer, and the high-mobility peak was identified as due to ions originating from the sprayed solution. Thus,  $\text{Na}^+(\text{H}_2\text{O})_n$  with  $n = 3-7$  were observed when aqueous solutions of NaCl were sprayed. These early mobility studies<sup>2,34</sup> can be considered as the first good experimental evidence for IEM.

Iribarne and Thomson<sup>34</sup> came to the conclusion that the formation of abundant high-mobility gas-phase ions is possible only if a considerable fraction of the charges (i.e., ions) escaped from the droplets before the complete evaporation of the droplets. The theory for this escape process, ion evaporation, was developed in the same paper.<sup>34a</sup>

### 1.2.9 The Iribarne–Thomson Equation for Ion Evaporation from Small Charged Droplets and Subsequent Experimental and Theoretical Work Examining the Validity of IEM

Iribarne and Thomson derived an equation that provided detailed predictions for the rate of ion evaporation from the charged droplets.<sup>34a</sup> The treatment is based on transition state theory, used in chemical reaction kinetics. The rate constant  $k_1$  for emission of ions from the droplets is given by

$$k_1 = \frac{k_B T}{h} e^{-\Delta G^\ddagger/kT} \quad (1.11)$$

where  $k_B$  is Boltzmann's constant,  $T$  is the temperature of the droplet, and  $h$  is Planck's constant. The free energy of activation,  $\Delta G^\ddagger$ , was evaluated on the basis of the model shown in Figure 1.7. The transition state selected by the authors resembles the products more than the initial state; that is, it is a “late” transition state. The advantage of this choice is that the energy of such a state can be expressed by a closed equation based on classical electrostatics and thermodynamics. However, the transition state could in reality be occurring earlier—for example, as the ion disrupts the droplet surface. The energy of such an early transition state would be much more difficult to evaluate. If a higher free energy barrier did occur at the earlier stage, the predictions of the Iribarne–Thomson model would be less sound.

The top of the barrier in the Iribarne–Thomson transition state is due to the opposing electrostatic forces: (a) the attraction between the escaping ion and the droplet, arising from the polarizability of the droplet, and (b) the Coulomb repulsion of the escaping ion by the remaining charges of the droplet. The ion-polarizability attraction is larger at short distances, but as the distance is increased, it falls off much faster than the Coulomb repulsion between the ion and droplet charges. The transition state (see Figure 1.7) occurs at a distance  $x = x_A$ , where the attractive and repulsive energies are equal.

The free energy due to these two electrostatic forces,  $\Delta G(E)$ , is not the only term that enters the  $\Delta G^\ddagger$  expression. An ion desolvation term,  $\Delta G_{\text{dsol}}^0$ , that is independent of  $x$ , is also involved. The desolvation free energy  $-\Delta G_{\text{dsol}}^0$  corresponds to the free energy required to desolvate the ion—that is, transfer the ion from a neutral droplet of the same size to the gas phase. For relatively strongly solvated ions like the alkali ions, the most favorable path is for the ion to take several solvent molecules with it. For small, stronger solvating ions like  $\text{Li}^+$ , more solvent molecules are taken by the core ion. Thus, for water as solvent, the lowest  $\Delta G_{\text{dsol}}^0$  occurs for  $\text{Li}^+(\text{H}_2\text{O})_7$ , while for the larger  $\text{Cs}^+$ , the minimum occurs for  $\text{Cs}^+(\text{H}_2\text{O})_5$  (see Table III in Tang and Kebarle<sup>35</sup>). This reference provides also literature sources for the solvation energies of different ions. The individual properties of the ion enter into the ion evaporation rate constant mainly through the  $\Delta G_{\text{dsol}}^0$  term.

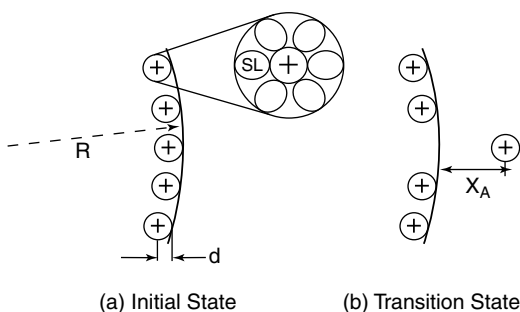


**Figure 1.7.** Model used in derivation of the Iribarne–Thomson equation. Part of surface of droplet with radius  $R$  is shown. (a) Excess of positive ions corresponding to the droplet charges located just below the surface. Each ion is solvated by several solvent molecules. (b) The transition state. Due to thermal activation, one of the ions has moved outside the droplet. (From Tang and Kebarle,<sup>35</sup> with permission from the American Chemical Society.)

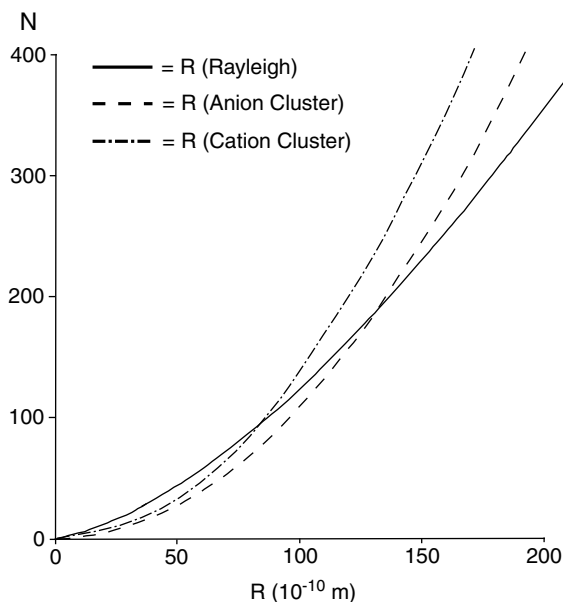


**Figure 1.8.** Predictions of the ion evaporation theory.<sup>34</sup> The Rayleigh curve provides the droplet radius  $R$  and the number of elementary charges  $N$  at which a charged water droplet will be at the Rayleigh limit. Moving at constant charge to a smaller radius  $R$  through solvent evaporation will cause a Coulomb fission. Similarly, the curves Cation Cluster and Anion Cluster show the threshold of ion evaporation at a given charge  $N$  and droplet radius  $R$ . For negatively charged droplets, moving at constant charge to a smaller radius  $R$  due to solvent evaporation will lead to negative ion evaporation when the radius  $R = 140 \text{ \AA}$  ( $1 \text{ nm} = 10 \text{ \AA}$ ) and for positively charged droplets at  $R = 84 \text{ \AA}$ , where the ion evaporation (Cation Cluster) and Rayleigh curves cross. Below this radius, ion evaporation replaces Coulomb fission. Thus taking a radius of  $R \approx 100 \text{ \AA}$  provides a useful benchmark for the region where ion evaporation takes over.

The curves shown in Figure 1.8, due to Iribarne and Thomson, summarize some of the predictions of the ion evaporation theory.<sup>34</sup> The initial charged droplets produced at the spray tip will lose volume by evaporation until they come close to the Rayleigh limit where the first Coulomb fission will occur. From then on, the droplet will experience repeated evaporation and fission events staying fairly close to the Rayleigh limit curve (as shown by experiments such as the results in Figure 1.4). Assuming that the droplets are positive, the + ion curve, crossing the Rayleigh curve,  $R(\text{Rayleigh})$ , at a radius  $R = 84 \text{ \AA}$ , ( $1 \text{ nm} = 10 \text{ \AA}$ ) indicates that ion evaporation will replace Coulomb fission at lower radii. As  $R$  decreases continuously by solvent evaporation, for radii smaller than  $R \approx 84 \text{ \AA}$ , there will be continuous loss of charge by ion evaporation, such that  $R$  and  $N$  follow exactly the  $R$  (cation cluster) curve. Because the  $\Delta G_{\text{dsol}}^0$  values entering the calculations leading to Figure 1.8 were not exactly known, it was suggested<sup>34</sup> that the crossing point for positive ions could be in the region of  $R = 70\text{--}120 \text{ \AA}$ . Thus, taking  $R \approx 100 \text{ \AA}$  provides a useful benchmark for the region where ion evaporation takes over.

While the Iribarne–Thomson equation provides a good conceptual description of the ion evaporation process, it has not proven useful for predictions of the observed relative intensities of ions in the ESI mass spectra. Iribarne and Thomson were interested only in relatively simple ions like the alkali ions. Even for these there can be ambiguities in the choice of the values of the parameters entering the ion evaporation equation.

Attempts were made<sup>35–37</sup> to examine the validity of IEM by evaluation of the ion evaporation rate constant  $k_1$  [see Eq. 1.11, where the  $\Delta G_{\text{dsol}}^0(\text{M}^+(\text{H}_2\text{O})_n)$  for ions like  $\text{Li}^+$ ,  $\text{Na}^+$ ,  $\text{K}^+$ , and so on, were obtained from experimental data in the literature. The rate constants  $k_1(\text{Li}^+)$ ,  $k_1(\text{Na}^+)$ , and so on, were compared with experimentally determined ion intensities,  $I(\text{Li}^+)$ ,  $I(\text{Na}^+)$ , and so on, when equal concentrations of the salts  $\text{LiX}$ ,  $\text{NaX}$ , and so on, were present in the solution. The observed ion abundance ratios should correspond to the evaluated rate constant ratios if IEM holds. The data used for the evaluation of  $\Delta G_{\text{dsol}}^0(\text{M}^+(\text{H}_2\text{O})_n)$  had error limits that led to some scatter of the evaluated  $\Delta G_{\text{dsol}}^0(\text{M}^+(\text{H}_2\text{O})_n)$  (see Table 1.1 in Kebarle and Peschke<sup>36a</sup>). The results showed a trend of decreasing free energy of activation,  $\Delta G^\ddagger(\text{M}^+)$  from  $\text{Li}^+$  to  $\text{Cs}^+$ , which should lead to increasing ion evaporation rate constants from  $\text{Li}^+$  to  $\text{Cs}^+$ .

Unfortunately, the experimentally observed ion abundances determined in different laboratories did not agree. Results from this laboratory<sup>36a</sup> showed similar intensities for the  $\text{Li}^+$ – $\text{Cs}^+$  series, while results from other laboratories such as Cole<sup>36c</sup> gave increasing intensities in the order  $\text{Li}^+$  to  $\text{Cs}^+$ , as expected on the basis of the calculated ion evaporation rate constants. The triple quadrupole mass spectrometer used in this laboratory<sup>36a</sup> exhibited large decreases of ion transmission with increasing  $m/z$ , and the corrections for the transmission changes used by Kebarle and Peschke<sup>36a</sup> could have been unreliable.

Fernandez de la Mora and co-workers<sup>29</sup> have used a different approach to provide strong evidence for the qualitative validity of the ion evaporation mechanism. They circumvent the difficulty caused by the so far impossible direct observation of the evolution of the very small rapidly evaporating droplets and the determination of their radius and charge. Instead, using solutions that contained a dissolved electrolyte, they focused on the sizes and charges of the solid residues formed after evaporation of the solvent. Since the solid residues had been “charged droplets” just before the last of the solvent evaporated, their sizes and charges represent, to a fair approximation, the sizes and charges of evolving charged droplets that are now frozen in time and thus amenable to measurement.

A first effort using this approach<sup>29a</sup> provided results and interpretation that were in agreement with IEM. Using very low flow rates and high conductivity (high electrolyte concentration) solutions, very small initial droplets were produced by ES. These droplets were chosen because they are expected to reach the Iribarne ion emission radius (if IEM holds) before experiencing Rayleigh disintegration. The mobility of the charged solid residues formed from such droplets was determined. The mobility depends on both the radius and the charge of the residues. The radius could be determined independently by using a “hypersonic impactor” apparatus that provides the mass of the residues. The radius was obtained by assuming that the density of the residues was the same as that of the solid salt. The charge of the residues was then deduced from the known mobility and the now known radius of the solid residue. The charge  $q$  determined for a given solid residue with known radius was found to be considerably lower than the charge  $q_{\text{Ry}}$  required by the Rayleigh stability equation. This finding is in agreement with the prediction of the Iribarne Ion Evaporation Theory that when the droplets reach a given small radius, ion evaporation requires a smaller overall charge than does Coulomb fission (see Figure 1.8).

These findings could be considered as a strong experimental support for IEM. However, an obvious objection is the assumption that the density of the residues is the same as the density of the solid salt. The morphology of the solid residues formed by ES could be much more complex than that of solid crystals of the salt, and thus the density of the residues could be lower. Additional work<sup>29b,c</sup> using more advanced experimental methodology removed some of the problems of the previous work,<sup>29a</sup> such as the problem of the unknown density

of the residues. For further details see Fernandez de la Mora and co-workers<sup>29b,c</sup> or a less technical, brief discussion in Kebarle.<sup>36b</sup>

Much greater problems in applying the Iribarne–Thomson equations are encountered with organic ions. Many of these can be surface-active, and even very weak surface activity is expected to have a very significant effect on the relative intensities observed with ESIMS. The surface activity will have a twofold effect on the ion evaporation rate constant: (a) The surface-active ions will be favored as charges at the surface of the droplets because they are surface-active. (b) The surface-active ions will have lower desolvation energies because the hydrophobic groups responsible for the surface activity are not well-solvated. Thus organic ions with higher surface activities will have higher ion evaporation rate constants. For a very effective use of surface activity of analytes, see the chapter by Cech and Enke (Chapter 2) in this volume.

Nohmi and Fenn<sup>38a,b</sup> have also provided experimental evidence that supports IEM.

Theoretical work involving simulations of ion evaporation from charged droplets can also provide valuable insights into IEM. A good example is the work by Vertes and co-workers<sup>38c</sup> on the evaporation of  $\text{H}_3\text{O}^+$  ions from charged water droplets. The authors used classical molecular dynamics simulations to study droplets of 6.5-nm diameter. Checks were made that the parameters used led to predictions of properties such as the radial distribution function, the enthalpy of evaporation, and the self-diffusion coefficients that are in agreement with experimental values. Droplets of 6.5-nm diameter, which have some 4000 water molecules, are expected to lose charges by IEM when charged to the Rayleigh limit (see Figure 1.8). The droplet was charged with  $\text{H}_3\text{O}^+$  ions, but ion pairs corresponding to a dissolved solute were not added. At equilibrium, not all  $\text{H}_3\text{O}^+$  ions were located on the surface of the droplet as generally assumed for IEM. The fluctuations of water molecules at the droplet surface became much more accentuated as the  $\text{H}_3\text{O}^+$  charges were added and some of these fluctuations developed into large protuberances that separated as hydrated  $\text{H}_3\text{O}^+$  ions. Generally, the “solvation shell” of the departing  $\text{H}_3\text{O}^+$  consisted of some 10 water molecules. Interested readers can observe the simulation of such ion evaporation at the website of Vertes: <http://www.gwu.edu/~vertes/publicat.html>.

In summary, the ion evaporation mechanism is experimentally well-supported for small inorganic and organic ions, but development of quantitative predictions based on this model remains a considerable challenge for the future.

### **1.2.10 Large Analyte Ions Such as Proteins and Dendrimers Are Most Probably Produced by the Charged Residue Model (CRM)**

Denatured and non-denatured globular proteins and protein complexes are routinely produced by ESI. Native proteins will, in general, remain folded when sprayed in a water–methanol solution—that is, at a neutral pH of  $\sim 7$ . However, some proteins may be very sensitive to the conditions used and denature partially. Denaturing is easily recognized from the observed mass spectrum. Folded (non-denatured) proteins lead to mass spectra consisting of a compact series of peaks that correspond to the molecular mass of the protein charged (in the positive ion mode) by a number  $Z$  of  $\text{H}^+$  ions. A small protein like lysozyme (Lys) is observed to lead to three peaks due to three different charge states with  $Z = 8, 9, \text{ or } 10$ . When the protein is denatured, the charge distribution is observed to be very broadened, covering a large number of peaks that extend to much higher charge states,  $Z$ . Obviously, it is of special interest to understand the mechanisms that lead to these observations.

An early study by R. D. Smith and co-workers<sup>38d</sup> provided good evidence that proteins are produced via CRM. If CRM holds, one would expect that when small charged droplets evaporate, there could be not only one protein, but also more than one protein, in the droplets. Therefore, one should observe in the mass spectra not only monomers, but also dimers, trimers, and higher multimers. The authors<sup>38d</sup> observed a preponderance of multiply charged monomers and much lower and rapidly decreasing intensities of dimers and trimers, where the charge to total mass ratio,  $z/m$ , value decreased with the degree of multimerization. Using a quadrupole mass spectrometer that had a very high mass range, the authors<sup>38d</sup> were able to observe even higher multimers and came to the conclusion that the results are consistent with CRM and a droplet evolution following a scheme of the type shown in Figure 1.6.

In later work, Smith and co-workers<sup>39a</sup> found an interesting empirical correlation between the molecular mass,  $M$ , and the average charge,  $Z_{av}$ , of starburst dendrimers [see Eq. 1.12]. These multibranched alkyl-amine polymers have relatively rigid structures that are close to spherical, with shapes resembling those of globular proteins. Results for non-denatured proteins were found also to fit Eq. 1.12.

$$Z_{obs} = aM^b \quad (1.12)$$

$Z_{av}$  is the observed average charge state and  $M$  is the molecular mass of the ion while  $a$  and  $b$  are constants. The value  $b = 0.53$  led to the best fit. Standing and co-workers<sup>39b</sup> observed an identical relationship for a large number of non denatured proteins, where the value of  $b$  was between 0.52 and 0.55. (The term “average charge state for proteins” was first introduced and defined by Wang and Cole.<sup>39c</sup>)

Independently, Fernandez de la Mora<sup>40</sup> using the dendrimer data<sup>39a</sup>, and including also additional data from the literature for non-denatured proteins, was able to show not only that the empirical relationship [Eq. 1.12] holds, but also that the relationship can be derived on the basis of the charged residue mechanism. The plot shown in Figure 1.9 is based on the data used by Fernandez de la Mora, but includes also the protein data of Ens and Standing.<sup>39b</sup>

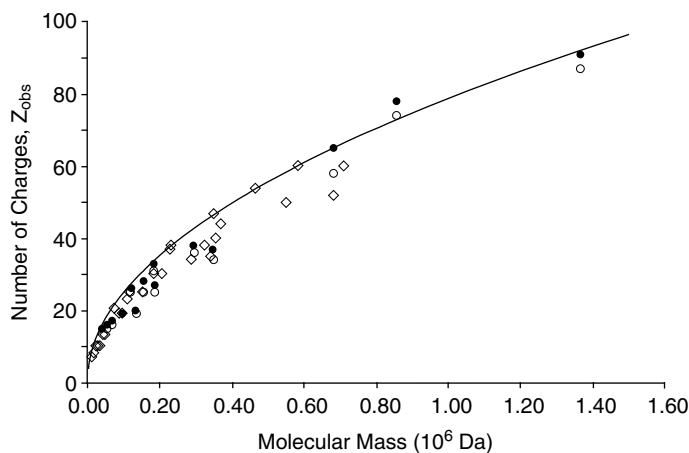


**Figure 1.9.** Reproduction of a plot used by Fernandez de la Mora<sup>40</sup> and extended to include also data by Ens and Standing.<sup>39b</sup>  $Z_{obs}$  is the number of charges observed on proteins produced by ESIMS under non-denaturing conditions. ((●) Highest charge; ((○) lowest charge in mass spectrum (Fernandez de la Mora<sup>40</sup>); ((◇) average  $Z_{obs}$  (Ens and Standing<sup>39b</sup>)). Solid curve corresponds to charge  $Z$  predicted by Eq. 1.1.2.

The derivation of Fernandez de la Mora<sup>40</sup> was based on the following arguments. There is theoretical<sup>40</sup> evidence that the evaporating charged droplets (which in the present context are assumed to contain one globular protein molecule) stay close to the Rayleigh limit. This is supported by more recent, experimental results<sup>25</sup> (see Figure 1.4b in Section 1.2.6) which involve charged evaporating water droplets of 35- to 5- $\mu\text{m}$  diameter. These show that the charge is approximately 95% of the Rayleigh limit when the droplets experience a Coulomb fission and approximately 75% of the Rayleigh limit immediately after the Coulomb fission. Thus, the droplets stay at all times within the limits of 95–75% of the Rayleigh limit, and both of these values are close to the Rayleigh limit. Fernandez de la Mora<sup>40</sup> reasoned that when the charged water droplet, containing one protein molecule, evaporates completely, the charges on the droplet will be transferred to the protein. He assumed also that the protein will be neutral when all the water is gone so that the charges on the surface of the droplet become the charge of the protein observed in the ESI mass spectrum of the protein.

The radius of the protein can be evaluated with Eq. 1.13, where  $\varphi$  is the density of the protein.

$$(4/3\pi R^3 \varphi) N_A = M \quad (1.13)$$

$N_A = 6 \times 10^{23}$  is the number of molecules per mole;  $R$  is the radius of the protein, and  $M$  is the molecular mass of the protein. Fernandez de la Mora assumed that the non-denatured proteins have the same density  $\varphi$  as water,  $\varphi = 1 \text{ g/cm}^3$ . Evidence in support of that assumption based on mobility measurements by Jarrold and Clemmer<sup>41a</sup> is given in Section 2.2 of Fernandez de la Mora.<sup>40</sup> The charge of the protein is taken to be the same as the charge of a water droplet of the same radius,  $R$ , that just contains the protein and is at the Rayleigh limit. The charge can be obtained by evaluating  $R$  with Eq. 1.13 and substituting it in the Rayleigh equation [Eq. 1.10] and expressing the charge,  $Q = Z \times e$ , where  $Z$  is the number of elementary charges and  $e$  is the value of the elementary charge. The result is given in Eq. 1.14:

$$Z = 4(\pi\gamma\epsilon_0/e^2 N_A \varphi)^{1/2} \times M^{1/2} \quad (1.14)$$

$$Z = 0.078 \times M^{1/2} \quad (1.14a)$$

where  $Z$  is the number of charges of the protein,  $\gamma$  is the surface tension of water,  $\epsilon_0$  is the electrical permittivity,  $e$  is the electron charge,  $N_A$  is Avogadro's number,  $\varphi$  is the density of water, and  $M$  is the molecular mass of protein. The constant 0.078 in Eq. (1.14a) gives the number of charges on a protein of molecular mass  $M$  in mega daltons.

The solid line in Figure 1.9 gives the predicted charge based on Eq. (14a). Good agreement with the experimental results is observed. Notable also is the predicted exponent of  $M$ , which is 0.5, while the exponent deduced from the experimental data<sup>39,40</sup> is 0.53. It should be mentioned that Fernandez de la Mora's treatment<sup>40</sup> was preceded by a similar but much less detailed proposal by Smith and co-workers.<sup>39a</sup>

The agreement of Eqs. 1.14 and (14a) with the observed charges  $Z$  can be considered as strong evidence that globular proteins and protein complexes are produced by the charged residue mechanism.

Most of the data points in Figure 1.9 were obtained not with neat water as solvent, but from solutions of water and methanol. These solutions are easier to use in ESIMS because neat water, due to its high surface tension, can initiate electrical gas discharges at the spray needle (see Section 1.2.4). Nevertheless, the surface tension of water,  $\gamma = 73 \times 10^{-3} \text{ (N/m)}$

(see Table 1.1), was used by Fernandez de la Mora<sup>40</sup> in Eq. 1.14 for the surface tension of the droplets. The surface tension of methanol,  $\gamma = 22.6 \times 10^{-3}$  (N/m), is much smaller. However, the assumption can be made that the evaporating droplets will lose methanol preferentially because methanol has a much higher vapor pressure, and therefore the final droplets that contain the protein will be very close to neat water droplets. This can be expected because there has been a very large loss of solvent by evaporation before the final very small droplets containing the protein are formed (see Figure 1.6 and associated discussion).

A recent compilation of data by Heck and van der Heuvel<sup>41d</sup> has shown that the square root dependence of the charge  $Z$  on  $M$  [see Eq. (14a)] holds also for protein complexes.

Fernandez de la Mora<sup>40</sup> did not consider the actual chemical reactions by which the charging of the protein occurs. These reactions will depend on what additives were present in the solution. Thus, in the presence of 1% of acetic acid in the solution, the charges at the surface of the droplets will be  $\text{H}_3\text{O}^+$  ions. Charging of the protein will occur by proton transfer from  $\text{H}_3\text{O}^+$  to functional groups on the surface of the protein that have a higher gas-phase basicity than  $\text{H}_2\text{O}$ . The gas-phase basicities are relevant because the solvent will essentially have disappeared. There are plenty of functional groups on the protein that have gas-phase basicities that are higher than that of  $\text{H}_2\text{O}$ . These could be basic residues or amide groups of the peptide backbone at the surface of the protein. Gas-phase basicities of several representative compounds are given in Table 1.4 in Section 1.2.12.

Recent results by Samalikova and Grandori<sup>42a</sup> have provided evidence that contradicts Fernandez de la Mora's CRM model. Solvents that have a lower surface tension than water should lead to lower charge states of the proteins, because the droplet charge at the Rayleigh limit [see Eq. 1.14] is proportional to the square root of the surface tension,  $\gamma$ . Use of solvents such as 1-propanol, with  $\gamma = 23 \times 10^{-3} \text{ N m}^{-1}$  compared to water  $\gamma = 73 \times 10^{-3} \text{ N m}^{-1}$ , should lead to a decrease of the observed charge by a factor of  $\sqrt{73/23} = 1.8$ . However, essentially no charge change was observed for the proteins (ubiquitin, cytochrome C, and lysozyme). The nonaqueous solvents that were used, such as 1-propanol, were not neat propanol but instead a solution containing some 30% propanol and 70% water (by volume). Grandori et al. made the assumption that the solvent with the higher vapor pressure ( $\text{H}_2\text{O}$  in the present case) evaporates first, leaving the less volatile solvent (1-PrOH) behind.

Samalikova and Grandori<sup>42</sup> were not the first investigators to use solvent mixtures involving water and another less volatile solvent with lower surface tension. Earlier work by Iavarone and Williams<sup>43</sup> also examined the effect of solvents with different surface tension on the charge states of macromolecules, such as dendrimers. Of special interest are their results for dendrimers because these have stable, close-to-spherical structures that are not affected by nonaqueous solvents. One of the solvents used was 2-propanol, which bears some similarity to the 1-propanol used by Samalikova and Grandori. For the DAB 60 dendrimer, they found the average charge to be  $Z_{\text{av}} = 2.63$  (propanol) and  $Z_{\text{av}} = 4.72$ , (water), which leads to  $Z_{\text{av}}/Z_{\text{Ry}} = 1.09$  for propanol and  $Z_{\text{av}}/Z_{\text{Ry}} = 0.98$  (water), in good agreement with the CRM<sup>40</sup> expected result. For the DAB 64 dendrimer, the  $Z_{\text{av}} = 7.6$  (2-propanol) was considerably smaller than  $Z_{\text{av}} = 9.9$  (water) as expected from CRM.<sup>40</sup> The ratios were  $Z_{\text{av}}/Z_{\text{Ry}} = 1.27$  (propanol) versus  $Z_{\text{av}}/Z_{\text{Ry}} = 0.9$  (water). Obviously the  $Z_{\text{av}}$  for 2-propanol is higher than it should be, but still acceptable as support for the CRM.

Iavarone and Williams<sup>44</sup> suggest that the lack of change of charge,  $Z_{\text{av}}$ , when a solvent of low surface tension is used, observed by Samalikova and Grandori, is caused by a conformational change of the proteins due to the presence of the nonaqueous organic solvent in the solution that was sprayed. Such a partial denaturing increases the size (radius  $R$ ) of the

protein and is thus expected to lead to a larger  $Z_{av}$ . The charge  $Z$  depends on  $R^{3/2}$ , while the dependence on the surface tension,  $\gamma$ , is much weaker,  $\gamma^{1/2}$ . Thus, it would take a relatively small change of  $R$ , due to unfolding, to compensate for the change of  $\gamma$ . Conformational changes of proteins caused by organic solvents have been well documented (see, for example, Karger and co-workers<sup>45</sup>). Evidence for partial unfolding of proteins, when alcohols were added to the solution used for ESIMS determinations, has been provided by Kaltashov and Mohimen.<sup>46</sup>

It is well known that denaturing of a protein introduces not only an increase of the charge state, but also a characteristic broadening of the charge state distribution. Examining the mass spectra in Figure 1.1 of Samalikova and Grandori,<sup>42a</sup> one finds significant broadening for cytochrome C and ubiquitin, but no broadening for lysozyme. Thus only lysozyme provides evidence that decrease of the surface tension does not lead to a decrease of  $Z_{av}$  as expected from Eq. 1.14 and the charged residue model. This result is significant and therefore, at this time, one cannot completely reject the Grandori results and interpretation. Clearly, additional work is desirable, such as (a) an examination of the reproducibility of the results<sup>42</sup> and (b) additional experiments with dendrimers in different solvents.

An extension of the charged residue model was provided recently by Kaltashov and Mohimen.<sup>46</sup> Determinations of ESI mass spectra and charge states of some 22 proteins extending in mass from 5 to 900 kDa were made, using the same experimental conditions in all measurements. In this manner, the authors<sup>46</sup> avoided having to use mass spectra from the literature that were obtained at a variety of conditions. Representative mass spectra for a small protein (insulin) and a large protein (human serum transferrin–transferrin receptor complex) are given in Figure 1.10, upper row. Both spectra show a narrow charge

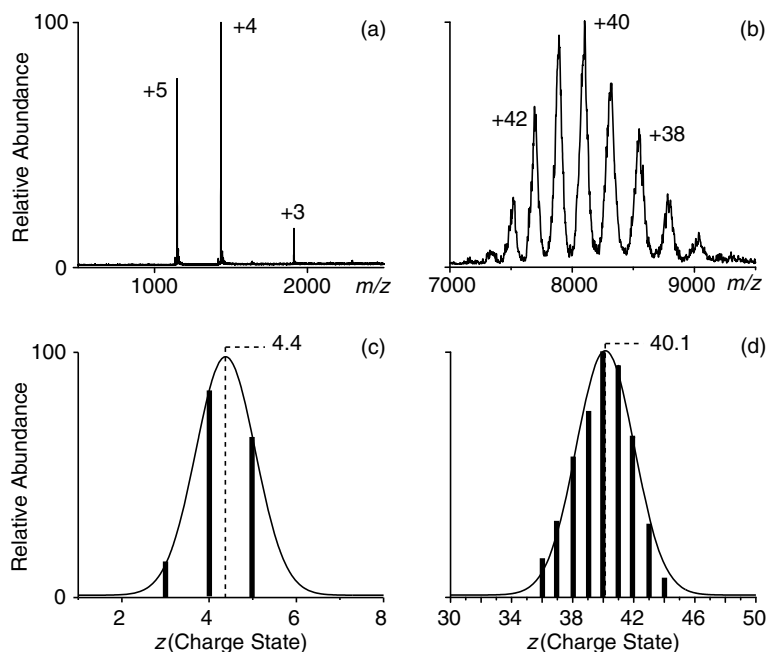


**Figure 1.10.** ESI mass spectra of insulin, A. Human serum transferrin-transferrin receptor complex, B. These spectra were used to calculate the average number of charges  $Z_{av}$  on the proteins, as illustrated with diagrams C and D. (Reprinted from Kaltashov and Mohimen,<sup>46</sup> with permission from the American Chemical Society.)

distribution indicating that the protein structures were not denatured. The average charge,  $Z_{av}$ , was determined by integration of the peaks as shown in Figure 1.10, lower row.

The authors<sup>46</sup> reasoned that the spherical approximation used by Fernandez de la Mora<sup>40</sup> is only seldom a realistic representation of the shape of native proteins. While the spherical shape provides a best fit for the spherical charged droplets, erroneous results are expected when the protein shape deviates from spherical. Therefore a better approach would be to use the protein surface area.

The correlation obtained with the surface area,  $S$ , of proteins evaluated from their known crystal structures and the charge states  $Z_{av}$ , obtained from the mass spectra of the 22 proteins, is shown in Figure 1.11. The fit of the data points [linear plot insert in Figure 1.11, corresponding to Eq. (15a)] is very much better than the fit in the Fernandez de la Mora<sup>40</sup> plot (Figure 1.9), which is based on the spherical protein approximation and  $Z_{av}$  data from different literature sources. The straight line obtained from the  $\ln$ - $\ln$  plot (Figure 1.11) can be represented by Eq. (15b), where  $\ln A$  is the intercept with the  $\ln Z_{av}$  axis and  $a$  is the slope of the straight line. The value  $a = 0.69$  is obtained from the plot.

$$Z_{av} = A \times S^a \quad (1.15a)$$

$$\ln Z_{av} = \ln A + a \ln S \quad (1.15b)$$

The authors<sup>46</sup> were able to show that the exponent  $a$  of the slope,  $S$ , could be derived if one assumes that the charging of the proteins occurred as shown in the schematic representation

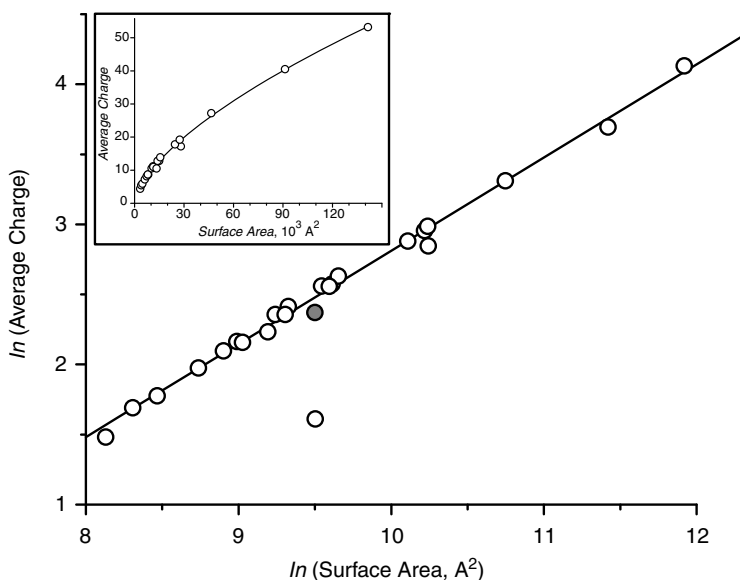


**Figure 1.11.** Correlation between average charge state of protein ions generated by ESI under near-native conditions (10 mM ammonium acetate, pH adjusted to 7) and their surface areas in solution whose calculation was based on their crystal structures. The data are plotted in  $\ln$  (natural logarithmic) versus  $\ln$  scale (a graph using linear scales is shown in the inset). A gray-shaded dot represents a data point for pepsin, and the open circle underneath represents the maximum charge expected for pepsin if the extent of multiple charging was limited by the number of basic residues within the pepsin molecule. (Figure and text reprinted from Kaltashov and Mohimen,<sup>46</sup> with permission from the American Chemical Society.)

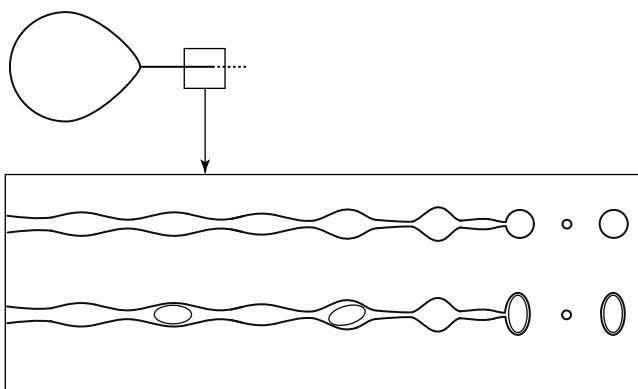


**Figure 1.12.** Schematic representation of a fission process for a droplet whose charge is equal to the Rayleigh limit. The straight line (jet) projecting from the pointed (cone) end of the droplet (top diagram) represents emission of a highly charged (at the surface) liquid, in the form of a jet. The axisymmetric disintegration of the jet is represented schematically in the boxed drawings. Capillary breakup in the absence of internal constraints produces two groups of homogeneous droplets (main and satellite). Presence of internal constraints in the stream (such as particles of a certain size) is likely to have a significant influence on the size and shape of the droplets. (Figure and text reprinted from Kaltashov and Mohimen,<sup>46</sup> with permission from the American Chemical Society.)

(Figure 1.12). A droplet at the Rayleigh limit emits a jet that separates into individual progeny droplets. The protein that escapes the parent droplet is shown to be fitting a progeny droplet. Under these conditions, the charging of the progeny droplets and the progeny that contains the protein will be determined by parameters associated with the formation of the jet.<sup>46,47</sup> These are different from the Rayleigh spherical droplet stability conditions. It is the former conditions<sup>46</sup> that lead to slope =  $a$ , which is in agreement with the experimental results (Figure 1.12).

It is interesting to see what type of fit to the Fernandez de la Mora equation [Eq. (14a)] is obtained with the proteins and their charges determined by Kaltashov and Mohimen.<sup>46</sup> A plot of the charge  $Z$  versus the molecular mass  $M$  is shown in Figure 1.13. The experimental points fit very well the curve obtained with Fernandez de la Mora's Eq. (14a),  $Z = 0.078 \times M^{0.5}$ . The fit is very much better than that observed in Figure 1.9 that used data obtained from several different laboratories. The best-fit curve to the data in Figure 1.13 leads to  $Z = 0.041 \times M^{0.547}$ . Considering the good visual fit in Figure 1.13, one could argue that the use of the surface area of the proteins is not an improvement. However, one experimental point<sup>46</sup>—that is, that for ferritin—provides clear evidence that the surface area counts. Ferritin in the Fernandez de la Mora plot (Figure 1.13) shows a large deviation to a higher charge, while in the surface area plot (Figure 1.11) there is no deviation. As pointed out by Kaltashov and Mohimen,<sup>46</sup> the apo-ferritin used is approximately spherical, but has a large cavity on one side, which increases the surface area substantially and causes the higher charge. For an informative discussion of Kaltashov and Mohimen's data, see Benesh and Robinson.<sup>47</sup>

In summary, the Charged Residue Mechanism has allowed quantitative predictions of the protein charge state in the gas phase and is well-supported for large proteins of widely varying mass. The rather simple assumptions at the basis of the mechanism have recently been examined and have led to the insight that proteins with large deviations from the spherical shape lead to better correlation of the charge with the surface of the protein.<sup>46</sup>

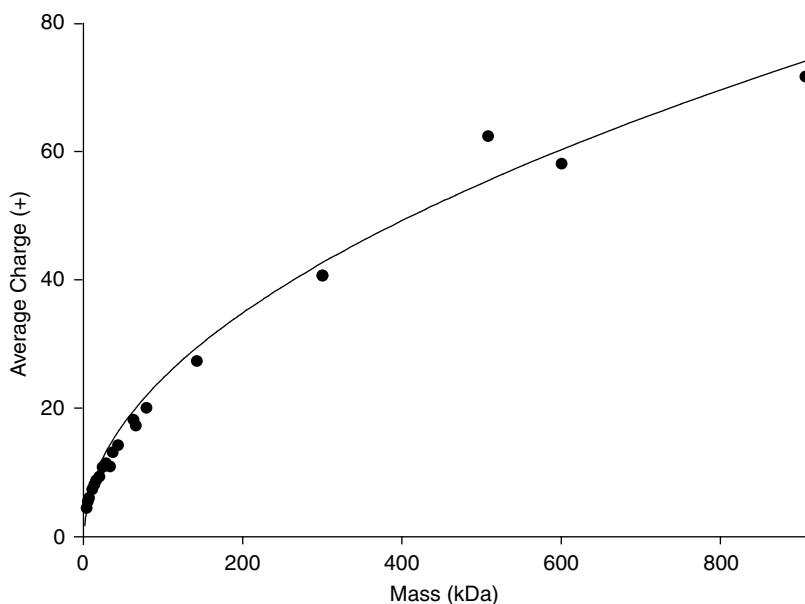


**Figure 1.13.** Plot of average charge of proteins observed by Kaltashov and Mohimen<sup>46</sup> versus molecular mass of protein. The solid line curve gives average charge predicted by the Fernandez de la Mora equation [Eq. 1.14]. A very good fit is observed except for one experimental point—that is, for ferritin (mass  $\approx$  510 kDa), which has a significantly higher charge  $Z$ . This protein is approximately spherical but has a cavity that increases its surface. This experimental point fits well in the charge versus protein surface plot (see Figure 1.11). (Figure 1.13 plot was graciously provided to the authors by Dr. Justin Benesh.)

The dependence on the surface of the protein and the model depicted in Figure 1.12 lend themselves to an extension. In solution, most of the ionized residues of native proteins are on the surface of the protein. When the protein approaches the surface of a positively charged larger droplet, several of the ionized basic residues of the protein may become part of the charge on the droplet. The specific shape of the protein and the closeness of the charges on the protein may introduce an instability of the droplet surface such that the droplet experiences a fission below the Rayleigh limit and the protein enters the first droplet of the cone jet caused by the fission. Because the surface-to-volume ratio increases as the droplet size decreases, this effect will become most important in the final stages of the droplet evolution when the droplets have become very small. Proposals that attachment of the protein to the surface of the droplet can introduce droplet instability and fission such that the protein leaves the droplet have been made before (see discussion of work by Karas and co-workers in Section 1.2.14). Some support for these models can be given also on the basis that proteins like pepsin that have only very few basic side chains are detected at very low sensitivities in the positive ion mode because the lack of positive sites reduces the ability of the protein to situate itself at the droplet surface.

It is notable that the generation of a charged protein in the gas phase by the above model falls somewhere between the CRM and the IEM. With CRM, the protein stays in the droplet until the solvent has evaporated and the charges of the droplet land on the protein. With IEM the protein leaves the droplet before it has evaporated, whereas in the model above, the protein stimulates the release of charged progeny droplets and leaves the parent drop in the first progeny drop that is of similar size to the protein.

### 1.2.11 Dependence of the Observed Ion Abundance of Analytes on the Nature of the Analyte, on Its Concentration, and on the Presence of Other Electrolytes in the Solution

The dependence of the sensitivities of different analytes observed with ESIMS on the nature of the analyte, on its concentration, and on the presence of other electrolytes in the solution is of interest both to the practicing experimental mass spectrometrists and to workers trying to relate the observations to the mechanism of ESI. The analytes considered in this section are not macromolecules like the proteins but are, instead, much smaller molecules that most likely enter the gas phase via the Ion Evaporation Model (IEM).

The dependence on various parameters of the total droplet current,  $I$ , produced at the spray capillary was given in Eq. 1.7. Relevant to the present discussion is the dependence of the current on the square root of the conductivity of the solution. At the low total electrolyte concentrations generally used in ESI, the conductivity is proportional to the concentration of the electrolyte. Thus, if a single electrolyte, E, was present, one would expect that the observed peak intensity,  $I_E$ , will increase with the square root of the concentration  $C_E$  [see Eq. 1.7]. Equation 1.7, is valid for the cone jet mode, which is used most often. At flow rates higher than the cone jet mode, the dependence on the concentration is lower than the 0.5 power.<sup>35</sup> Because ESIMS is a very sensitive method and the detection of electrolytes down to  $10^{-8}$  M is easily feasible, one seldom works with a one-electrolyte system. In general, even with a single analyte ion,  $A^+$ , there will be most often also impurity electrolyte EX present, where the  $E^+$  ions are generally  $Na^+$  and  $NH_4^+$  at levels below  $10^{-5}$  M. Therefore, there are two concentration regimes for the analyte:

- $C_A$  much higher than  $C_E$ . In that case, the  $I_A$  is expected to increase with the square root (or slower) of  $C_A$ .
- $C_A$  much smaller than  $C_E$ . In that case, the  $I_A$  is expected to increase with the first power of  $C_A$  because now  $I_A$  will depend on a statistical competition between  $A^+$  and  $E^+$  for being charges on the droplets.

To cover both regions, Tang and Kebarle<sup>35</sup> proposed Eq. (16a) for a two-component system in the positive ion mode.

$$\text{Two components:} \quad I_{A^+} = pf \frac{k_A C_A}{k_A C_A + k_E C_E} I \quad (1.16a)$$

$$\text{Three components:} \quad I_{A^+} = pf \frac{k_A C_A}{k_A C_A + k_B C_B + k_E C_E} I \quad (1.16b)$$

Equation (16b) is for three components:  $A^+$ ,  $B^+$ , and  $E^+$ .  $C_A$ ,  $C_B$ , and  $C_E$  are the concentrations in the solution,  $I$  is the total electrospray current leaving the spray capillary,  $I$  can easily be measured (see Figure 1.1), and  $p$  and  $f$  are proportionality constants (see Tang and Kebarle<sup>35</sup>) while  $k_A$ ,  $k_B$ , and  $k_E$  are the sensitivity coefficients for  $A^+$ ,  $B^+$ , and  $E^+$ , which depend on the specific chemical ability of the respective ion species to become part of the charge on the surface of the droplet and, once there, to enter the gas phase.

In the regime where  $C_A \ll C_E$ , Eq. (16a) reduces to Eq. (16c).

$$I_A = \text{const} \times C_A, \quad \text{where const} = k_A I_E / k_E C_E \quad (1.16c)$$

The experimental results<sup>35</sup> shown in Figure 1.14 give an example of a two-component system where the protonated morphine,  $MorH^+$ , is the analyte A, used at different

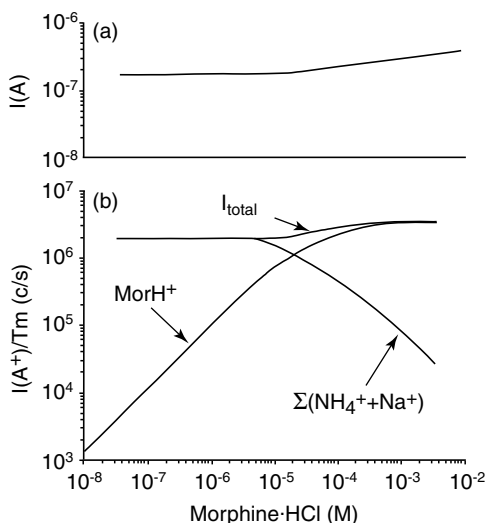


**Figure 1.14.** (A) Total electrospray current (Amp) with increasing concentration of analyte morphine · HCl. Due to presence of impurity ions ( $\text{Na}^+$  and  $\text{NH}_4^+$ ) at  $10^{-5}$  M,  $I_{\text{total}}$  remains constant up to the point where the analyte reaches concentrations above  $10^{-6}$  M. (B) Analyte  $\text{MorH}^+$  ion intensity (corrected for mass-dependent ion transmission,  $T_m$ , of quadrupole mass spectrometer used) is proportional to concentration of morphine · HCl up to the point where the morphine · HCl concentration approaches concentration of impurity ions. (Reprinted from Tang and Kebarle,<sup>35</sup> with permission from the American Chemical Society.)

concentrations, and the impurity ions  $\text{NH}_4^+$  and  $\text{Na}^+$ , present at constant concentrations, are the electrolyte,  $E$ . The observed linear region of  $\text{MorH}^+$  in the log–log plot used has a slope of unity at low concentrations,  $10^{-8}$ – $10^{-5}$  M, which means that the  $\text{MorH}^+$  ion is proportional to the morphine concentration. This region is suitable for quantitative determinations of analytes. At about  $10^{-5}$  M the increase of the  $\text{MorH}^+$  intensity slows down because the  $\text{MorH}^+$  concentration used comes close to that of the impurity electrolyte. Above that region where  $\text{MorH}^+ \text{Cl}^-$  becomes the major electrolyte, the peak intensity of  $\text{MorH}^+$  can grow only with the square root, or even a lower power, of the electrolyte concentration.

Expanding the system to three components, two analytes and the impurity  $E$ , leads to an unexpected result (see Figure 1.15). In this experiment the concentrations of the two analytes  $A = \text{tetrabutyl ammonium}$  and  $B = \text{cocaine}$  (upper figure) or  $\text{codeine}$  (lower figure) are increased together such that  $C_A = C_B$ . The impurity  $C_E$  is constant. The experiment was made in order to determine the relative sensitivities,  $k_A$  and  $k_B$ , of  $A$  and  $B$ . In the log–log plot used, the difference  $\log I_A - \log I_B$  equals the difference  $\log k_A - \log k_B$  and one would expect that the difference will be constant for  $C_A = C_B$  concentrations. However, this is not the case. The difference is constant only at high  $C_A = C_B$  concentrations and becomes zero at low concentrations.

The tendency of  $k_A/k_E$  to approach unity at low  $C_A, C_B$  indicates<sup>35</sup> that there is a **depletion** of the ion that has the higher sensitivity  $k$ . This is the ( $A = \text{tetrabutyl ammonium}$ ) ion in the present example. At  $C_A = C_B \ll 10^{-5}$  M, the current  $I$  and the total charge  $Q$ , of the droplets and the number of charged droplets are maintained by the presence of the electrolyte,  $E$ , whose concentration is much higher. Under these conditions, ionic species like  $A^+$  and  $B^+$ , when present at very low concentrations but having large coefficients  $k_A$  and  $k_B$ , find plenty of droplet surface to go to and ion evaporate rapidly. This results in a depletion of their concentration in the interior of the droplet. The ion  $A$  of higher sensitivity is depleted more than  $B$ , and this leads to an apparent value  $k_A/k_B = 1$ .

Experimental determination of the coefficient ratios  $k_A/k_B$  were performed<sup>35</sup> for a number of analytes in methanol by working at high concentrations  $C_A/C_B$ , where Eq. (16c) holds. The results in Figure 1.15 at high concentration represent two such determinations. It was found that the singly charged inorganic ions  $\text{Na}^+$ ,  $\text{K}^+$ ,  $\text{Rb}^+$ ,  $\text{Cs}^+$ ,  $\text{NH}_4^+$  had low

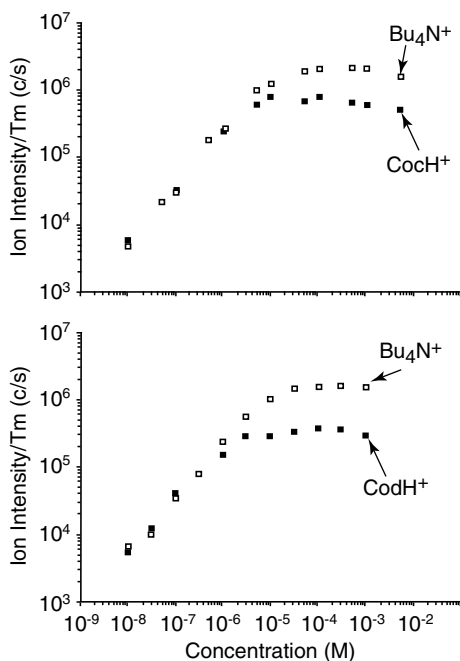


**Figure 1.15.** Ion intensities (corrected for mass-dependent ion transmission,  $T_m$ , of quadrupole mass spectrometer used) for pairs of analytes at equal concentration in solution. The different ESI sensitivities of the analytes are observable only at high analyte (above  $10^{-5}$  M) concentrations. (Reprinted from Tang and Kebarle<sup>35</sup> with permission from the American Chemical Society.)

sensitivity coefficients, while analyte ions that were expected to be enriched on the droplet surface (i.e., which were surface-active) had high coefficients that increased with the surface activity of the ions. Thus, assuming that  $k_{Cs}^+ = 1$ , the relative values  $k_A$  for the ions were:  $Cs^+ \approx 1$ ;  $Et_4N^+ = 3$ ;  $Pr_4N^+ = 5$ ;  $Bu_4N^+ = 9$ ;  $Pen_4N^+ = 16$ ;  $heptNH_3^+ = 8$ , where Et, Pr, Bu, and so on, stands for ethyl, *n*-propyl, *n*-butyl, and so on (see Table I in Tang and Kebarle<sup>35</sup>). The tetraalkyl ammonium salts and alkylammonium salts, and especially those with long chain alkyl groups, are known surfactants.

Assuming that IEM holds, ions from the droplet surface will leave the droplets and become gas-phase ions. In this case, the gas-phase ion sensitivity coefficient,  $k_A$ , for ions  $A^+$  will depend on the relative surface population of the droplet surface—that is, on the surface activity of ions  $A^+X^-$  given by a surface activity equilibrium constant  $K_{SA}$ —and on the rate constant for ion evaporation. The rate constant for ion evaporation is also expected to increase with the surface activity of the ion, because surface-active ions have low solvation energies (see Section 1.2.8). A third effect can be expected also. The very small droplets that lead to ion evaporation will, in general, be first- or second-generation progeny droplets (see Figure 1.6). Because the progeny droplets have higher surface-to-volume ratios relative to the parent droplets, an enrichment of the surface active ions is expected for the progeny droplets.

More recent work by Enke<sup>48</sup> made very significant advances starting from somewhat different premises. The role of the ion currents  $I, I_A$ , and so on, was represented by the molar concentrations of the ions. Thus the role of  $I$  was replaced with  $[Q]$  moles of charge and the role of the currents  $I_A, I_B, \dots$  was replaced by the molar concentrations of charges on the droplets due to the given ion species. Thus,  $[A^+]_S$  is the molar concentration of charges on the surface of droplets due to  $A^+$  species, and so on. The analyte  $A^+$  was assumed to distribute itself between the interiors of the droplets with a concentration  $[A^+]_I$  and as charge on the surface of the droplets  $[A^+]_S$ . An equilibrium between  $[A^+]_S$  and  $[A^+]_I$  was

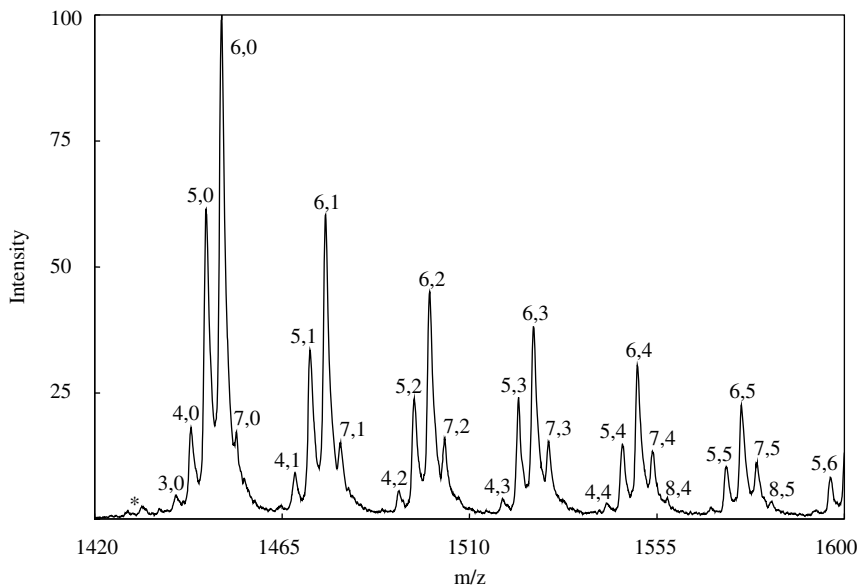


**Figure 1.16.** Mass spectrum of the major  $Z = +6$ , charge state of ubiquitin obtained from an aqueous solution of  $25 \mu\text{M}$  ubiquitin containing  $1 \text{ mM}$  NaI. In the absence of NaI, essentially only one peak is observed corresponding to ubiquitin +  $6\text{H}^+$ . The observed first group of peaks corresponds to ubiquitin, where the  $\text{H}^+$  charges are gradually replaced with  $\text{Na}^+$ . The largest peak in the first group, labeled 6,0, corresponds to ubiquitin +  $6\text{Na}^+$ . The second group has the same composition as the first group, but each ion contains also one  $\text{Na}^+$  and one  $\text{I}^-$ . The next group contains two  $\text{Na}^+$  and two  $\text{I}^-$ , and so on. The number  $n$  of  $\text{Na}^+$  ions is indicated with the first number over the peak, while the number  $m$  of  $\text{Na}^+\text{I}^-$  is given by the second number. (From Verkerk and Kebarle,<sup>58a</sup> with permission from Elsevier.)

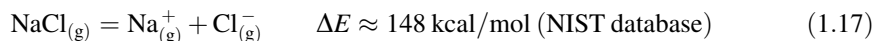
assumed. The other electrolytes were treated in the same way. Introduction of equations of charge balance and mass balance for each electrolyte led to an equation that predicts values for  $[\text{A}^+]_s$ ,  $[\text{B}^+]_s$ , and so on, on the basis of the parameters  $[\text{Q}]$ , which is known [see Eq. 1.3, the constants  $K_A$ ,  $K_B$ , and so on, and the concentrations  $C_A$ ,  $C_B$ , and so on. The assumption was made that  $[\text{A}^-]_s$ ,  $[\text{B}^+]_s$ , and so on, will be converted to gas-phase ions and are therefore proportional with the same proportionality constant,  $pf$  [see Eq. (16)], to the ion currents  $I_A$ ,  $I_B$ , and so on. The equation of  $[\text{A}^+]_s$ ,  $[\text{B}^+]_s$ , and so on, is of the same form as Eq. (16) in the high concentration range but not in the low concentration range. By taking into account, via mass balance, the depletion of the concentration  $C_A$  and  $C_B$  of the analytes with high coefficients  $k_A = K_A$ ,  $k_B = K_B$ , the equation of Enke provides an excellent fit of the ion abundance curves over the full concentration range, preserving a constant  $k_A/k_B$  ratio. Further development by Enke and co-workers has led to a most successful formalism (see Chapter 2, this volume).

### 1.2.12 Noncovalent and Ionic Interactions in Solution and in the Gas Phase and other Relevant Differences Between Gas Phase and Solution

In ESIMS the analytes experience both solution and gas-phase conditions, and therefore the mass spectrum of the analyte will reflect both gas- and solution-phase conditions. Many

practitioners of ESIMS with a biochemical background are well-acquainted with non-covalent and ionic reactions in aqueous solution, but don't have a strong background in gas-phase interactions. The present section provides a brief comparison of the interaction in the liquid and gas phase.

Whereas in water, the separation of an ion pair such as NaCl is spontaneous, in the gas phase, the separation requires the very large energy input of 148 kcal/mol, a value much larger than the energy required to break a C–C or a C–H covalent bond.



The binding energy increases when the positive and negative ions are small such as LiF, and it decreases for large ions such as CsI. A salt like NaCl is very soluble in water because of the very strong solvation interactions of the  $\text{Na}^{+}$  and  $\text{Cl}^{-}$  with the water molecules.

Very nonpolar compounds like the hydrocarbons are very weakly soluble in water, because the highly polar and hydrogen bonding water molecules interact very strongly with each other and thus exclude the hydrocarbon molecules.<sup>50</sup> The hydrocarbon molecules have weak van der Waals interactions with water molecules and somewhat stronger van der Waals interactions with each other. At very low concentrations of the hydrocarbon in water, this leads to formation of hydrocarbon islets in the water medium. Higher hydrocarbon concentrations lead to formation of two separate liquid phases.

Unfolded (i.e., denatured) proteins have regions that are hydrophobic and other regions, particularly where the ionized residues are located, which are strongly hydrophilic. The denatured protein will tend to fold spontaneously, such that the ionic residues face and interact with the water molecules while the hydrophobic sections interact with each other.

When charged analytes such as proteins are present in the evaporating droplets, ions such as  $\text{Na}^{+}$ , due to salt impurities, will begin to ion pair with the ionized acidic residues of the protein. This ion pairing will be driven by the very large loss of solvent by evaporation from the droplets. The bonding of these ion pairs is so strong that no amount of collision energy provided in the clean-up stages of the interface leading to the mass analysis region can remove these undesired  $\text{Na}^{+}$  adducts. Examples of such ion pairing effects are given in Section 1.2.13.

The gas-phase positive ions such as the alkali ions  $\text{Na}^{+}$  and  $\text{K}^{+}$  form fairly strongly bonded adducts with polar as well as aromatic compounds B. The bond dissociation energies<sup>51–55</sup> corresponding to the reaction



for a number of such ion–ligand complexes are given in Table 1.3.

Of special interest are ligands that model functional groups of proteins. For example, *N*-methylacetamide, which models the amide groups  $-\text{CH}_2\text{CONH}-\text{CH}_2-$  of the protein backbone, forms a bond with  $\text{Na}^{+}$  that is equal to 36 kcal/mol. Comparing this with the value for acetone, which is 30 kcal/mol,<sup>53</sup> the stronger interaction with the methylacetamide must be due to a contribution of the  $-\text{NH}_2-$  group. For the amino acids serine and proline, the binding energy ( $\sim 45$  kcal/mol) is even higher, probably due to participation of neighboring groups. These high values indicate that  $\text{Na}^{+}$  adducts to the amide groups of the proteins also will not dissociate in the clean-up stages of the ESI mass spectrometer. Thus, the presence of  $\text{Na}^{+}$  impurity in the solution is very undesirable because the mass shift due to the addition of  $\text{Na}^{+}$  to ionized acidic residues and to the amide groups of the protein interferes with the interpretation of the mass spectrum.

**Table 1.3.** Bond Enthalpies,  $\Delta H_{\text{B}}^0$ , for Reaction:  $\text{M}^+ \text{B} = \text{M}^+ + \text{B}$ 

$\text{M}^+$	$\text{H}_2\text{O}$	$\text{NH}_3$	Iso-PropOH	Acetamide	<i>N</i> -Methyl acetamide	Serine	Proline
$\text{Na}^+$	22.1 <sup>c</sup>	25.6 <sup>c</sup>	27.0 <sup>e</sup>	35.6 <sup>c</sup>	38.0 <sup>d</sup>	45.0 <sup>c</sup>	44.2 <sup>c</sup>
$\text{K}^+$	16.9 <sup>b</sup>	17.8 <sup>b</sup>	—	—	—	—	—

<sup>a</sup>All values in kmol/mol at 298 K.  $\Delta H_{\text{B}}^0$  value only weakly sensitive to temperature. For additional data on  $\text{Na}^+ \text{B}$  complexes see Ref. 50, and for  $\text{K}^+ \text{B}$  complexes see Refs. 50 and 52.

<sup>b</sup> Davidson and Kebarle.<sup>51</sup>

<sup>c</sup> Hoyau, et al.<sup>53</sup>

<sup>d</sup> Klassen et al.<sup>54</sup>

<sup>e</sup> Armentrout and Rodgers.<sup>55</sup>

The charging of an analyte such as a protein in the vanishing droplets will involve the excess charges at the surface of the droplets. When the solvent is a mixture of water and methanol, the methanol will have evaporated from the droplet; and if the droplet was at a somewhat acidic pH, due to the presence of millimolar acetic acid, the charging of the protein will involve proton transfer from  $\text{H}_3\text{O}^+$  to basic residues and the amide groups of the protein.

The gas-phase basicities of the solvent molecules ( $\text{H}_2\text{O}$  in the present case) and of compounds modeling functional groups of the protein are expected to determine the outcome of the proton transfer reaction. Table 1.4 provides gas-phase basicity data for several representative compounds.<sup>49</sup> Gas-phase basicity data for thousands of compounds are available on the NIST database.<sup>49</sup> The reaction rate constants of the vast majority of ion molecule reactions in the gas phase such as proton transfer or ligand transfer can be predicted on the basis of the thermochemistry of the reactions.<sup>56</sup> Thus, for example, the proton transfer reaction  $\text{AH}^+ + \text{B} = \text{A} + \text{BH}^+$  will proceed at collision rates, that is, without activation energy when the reaction is exoergic, that is, when the gas-phase basicity  $\text{GB}(\text{B})$  is greater than  $\text{GB}(\text{A})$ . The absence of activation energy is due to the attraction between the charge of the ion and the polarizable molecule. This attraction leads to a “collision” where the ion and molecule spiral around their center of mass until they collide with each other. These spiraling collisions lead to rate constants that are very large and can be evaluated with an equation based on Langevin’s work.<sup>56</sup> Furthermore, the energy released by the “collision” is sufficient to activate the reaction.<sup>56</sup>

**Table 1.4.** Gas-Phase Basicities of Bases B

$\text{GB}(\text{B})^a = \Delta G_{298}^0$ for reaction: $\text{BH}^+ = \text{B} + \text{H}^+$			
$\text{H}_2\text{O}$	157.7	$\text{NH}_3$	195.7
$(\text{H}_2\text{O})_2$	181.2	$\text{CH}_3\text{NH}_2$	206.6
$\text{CH}_3\text{OH}$	173.2	$\text{C}_2\text{H}_5\text{NH}_2$	210.0
$(\text{CH}_3\text{OH})_2$	196.3	$(\text{CH}_3)_2\text{NH}$	214.3
$\text{C}_2\text{H}_5\text{OH}$	178.0	<i>n</i> -PropNH <sub>2</sub>	211.5
$\text{CH}_3\text{CN}$	179.0	<i>N</i> -Methyl acetamide	205.0
$(\text{CH}_3)_2\text{O}$	182.7	Pyridine	214.8
$(\text{C}_2\text{H}_5)_2\text{O}$	191.0		

<sup>a</sup>  $\text{GB}(\text{B})$  = Gas-phase basicity. Values in kcal/mol.

All values from NIST Databases.<sup>50</sup> Often used are also the proton affinities. They correspond to the  $\Delta H^0$  value for the gas-phase reaction  $\text{BH}^+ = \text{B} + \text{H}^+$ .

Proteins, in general, will be easily protonated because they have basic residues with relatively high GBs. Thus GB(lysine) modeled by GB(*n*-propyl amine) = 212 kcal/mol (Table 1.4) has a much higher GB than GB((H<sub>2</sub>O)<sub>2</sub>) = 181 kcal/mol, and a proton transfer to lysine is expected. Proton transfer to the backbone amide group modeled by GB(N-methylacetamide) = 205 kcal/mol is also expected. In the statements above, we have assumed that the proton donors in the proton transfer are H<sub>2</sub>OHOH<sub>2</sub><sup>+</sup> species at the surface of the droplet. This is a plausible assumption, particularly if the charged residue model (CRM) holds.

On the other hand, protonation of a sugar-like glucose is unlikely because GB(glucose), roughly modeled by GB(ethanol) = 178 kcal/mol (Table 1.4), is too low. Experimentally, it was observed already quite early<sup>57</sup> that good ESI mass spectra of carbohydrates can't be obtained by protonation. However, spectra could be obtained by sodiation, achieved by the addition to the solution of mM concentrations of sodium acetate.<sup>57</sup> The sodium result is not surprising. Binding energies of sodium ions to sugars and even monosaccharides such as glucose do not seem to have been determined. However, high sodium affinities are expected because hydroxy groups on adjacent carbon atoms are present, which will lead to bidentate interactions with the sodium ion.

The gas-phase basicities and bond affinities such as in Tables 1.3 and 1.4 should be applied to charging of the analytes by the ion charges on the surface of the evaporating droplets with caution because of the complexity of the actual process that involves also a liquid surface. The application of the gas-phase data is much more straightforward for true gas-phase ion–molecule reactions that occur in the atmospheric region before the sampling capillary (or orifice) leading to the MS interface and in the following low-pressure stage before the skimmer (see Figure 1.2). Typically, these could involve charged solvent molecule clusters and analyte molecules, particularly when a countercurrent gas such as nitrogen was not used (see Figure 1.2). Such reactions are considered elsewhere (see Chapter 2, this volume).

### 1.2.13 Some Examples of Effects on Mass Spectra of Proteins Due to the ESI Process

#### 1.2.13.1 Ion Pairing of Salt Ions with Ionized Residues of Proteins

As discussed in the preceding sections and specifically Section 1.2.12, the formation of the gas-phase analyte ions occurs only after a very large loss of solvent from the charged droplets is produced by electrospray. This is the case for both mechanisms, CRM and IEM. In the presence of salts in the solution, the increase of concentration with solvent loss will lead to pairing of the positive with negative ions. This pairing will start long before all the solvent has evaporated. Pairing with salt ions will also involve ionized sites of the protein, that is, the ionized acidic and basic residues.

The pairing is most clearly observed in the mass spectrum when certain salts are used. One such salt is NaI. Shown in Figure 1.16 is the spectrum of folded ubiquitin obtained<sup>58a</sup> using nanospray of an aqueous solution containing 25 μM ubiquitin and 1 mM NaI. The Z = + 6 charge state is shown. This is by far the major charge state observed for ubiquitin.<sup>58a</sup> A series of groups of peaks containing Na and NaI is observed, and the composition of these ions is given in the figure caption. The observed composition can be rationalized by the operation of two processes: (a) replacement of the H<sup>+</sup> charges with Na<sup>+</sup> charges where the Na<sup>+</sup> come from the surface of the droplets such that the ultimate charging of the protein involves exclusively Na<sup>+</sup> rather than H<sup>+</sup> charges and (b) ion pairing of Na<sup>+</sup> ions in the

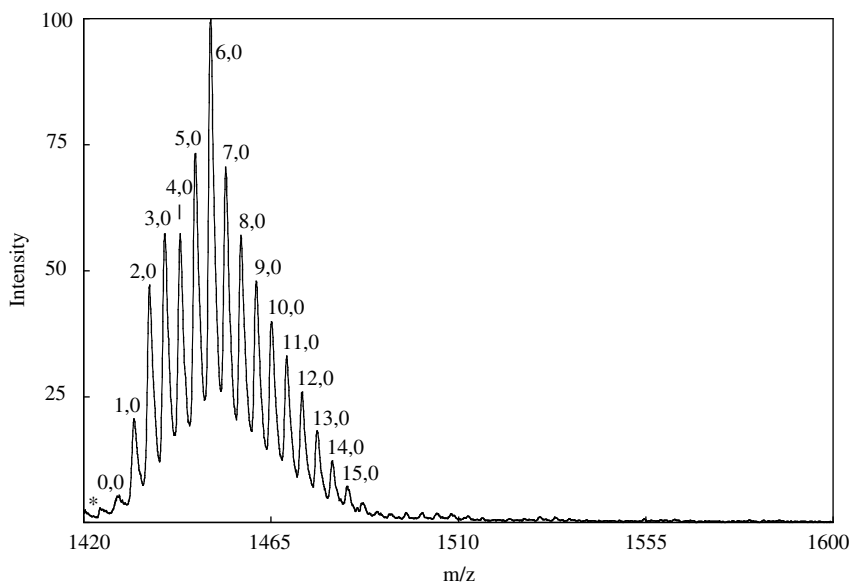
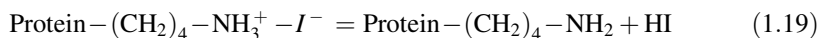


**Figure 1.17.** Mass spectrum of ubiquitin  $Z=6$  charge state under the same conditions as in Figure 1.16 but at high collisional activation (CAD). All the peaks that contained  $\text{Na}^+ + \text{I}^-$  pairs have disappeared and are replaced by uncharged Na adducts. This process is consistent with loss of HI where the  $\text{I}^-$  ions paired to an ionized basic residue dissociated as HI. (From Verkerk and Kebarle,<sup>58a</sup> with permission from Elsevier.)

solution of the droplet with ionized acidic residues and  $\text{I}^-$  with ionized basic residues at the surface of the protein.

The spectrum (Figure 1.16) was obtained at low nozzle (spray capillary) to skimmer potential, so that there was little collisional activation of the protein. At a high potential, multiple loss of HI was observed (see Figure 1.17). All the peaks that contained  $\text{Na}^+ + \text{I}^-$  pairs have disappeared and were replaced by peaks with unpaired Na adducts.

The observations based on Figures 1.16 and 1.17 can be rationalized as follows: (a) *Charging* reactions by  $\text{Na}^+$ . The sodium ion goes either on ionized acidic residues or on the amide groups of the protein back bone. The  $\text{Na}^+$  bonding at both these sites is strong (see Table 1.3), and therefore no loss of Na is expected even at high CAD conditions. (b) Ion pairing reactions involving both  $\text{Na}^+$ , going to same sites as in (a), and  $\text{I}^-$ , going predominantly to the ionized basic residues. *No charging* occurs. At high CAD conditions, HI is formed by reaction 1.19, where the basic residue shown is lysine:



Experiments involving the salts NaCl and NaAc, where Ac stands for the acetate anion, were made and it was found<sup>58</sup> that the energy required for the dissociation decreased in the order HI, HCl, HAc. It was also shown,<sup>58a</sup> on the basis of theoretical data, that this order is expected and the energy required is well within the range provided by the CAD used.

Additional evidence that the basic side chains are involved in the dissociation reaction was obtained by experiments where much higher concentrations of sodium acetate were added so as to be certain that all the ionized acidic sites were paired with  $\text{Na}^+$  and all basic sites with the acetate anions. The mass spectrum of the  $Z=6$  charge state for ubiquitin and sodium acetate at high CAD is shown in Figure 1.18. The sharp break of peak intensity past

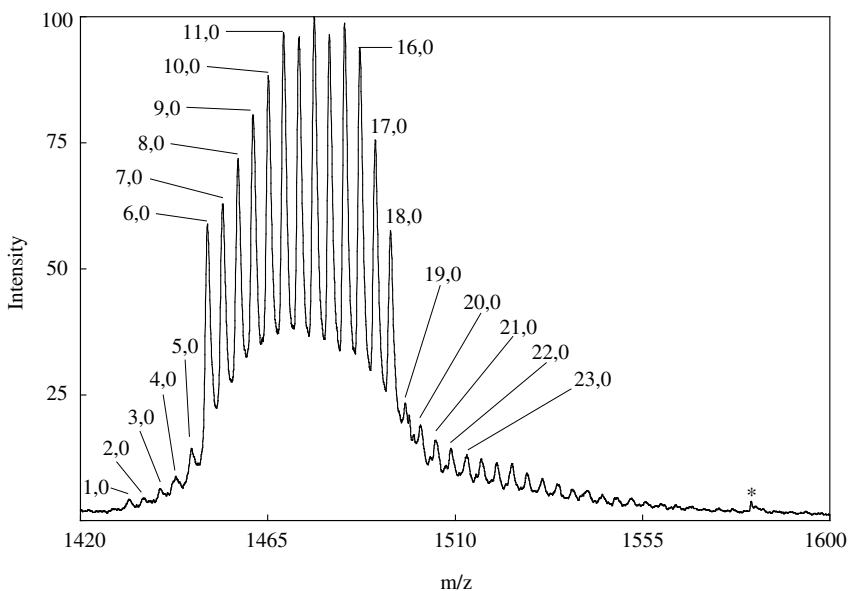
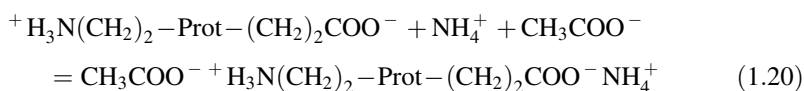


**Figure 1.18.** Mass spectrum showing  $Z=6$  charge state obtained with ubiquitin (25  $\mu\text{M}$ ) and a high (5 mM) concentration of sodium acetate at high CAD where all acetate anions have fallen off as acetic acid molecules. The sharp break of peak intensity past  $n=18$  indicates that the observed ubiquitin has 6  $\text{Na}^+$  charges and 12 ionized acidic sites on the protein which are sodiated. (From Verkerk and Kebarle,<sup>58a</sup> with permission from Elsevier.)

$n=18$  indicates that the observed ubiquitin has 6  $\text{Na}^+$  charges and 12 ionized acidic sites paired to  $\text{Na}^+$  ions, giving a total of  $n=18$ . The acetate anions that had ion paired with the ionized basic sites have fallen off as acetic acid in a reaction analogous to Eq. 1.19. An examination of the number of acidic residues and the terminal acidic group of ubiquitin showed a total number of 12 acidic sites and all of these were near the surface of the protein, in agreement with the proposed ion pairing mechanism.<sup>58a</sup>

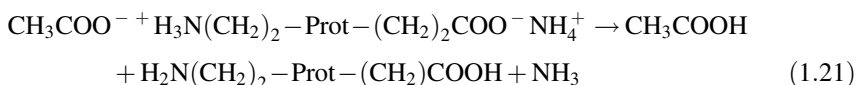
### 1.2.13.2 Why Is Ammonium Acetate Such a Popular Salt Additive to Solutions Used for ESIMS<sup>58a</sup>

Ammonium acetate at millimolar concentrations is very often used as an additive to solutions, particularly so when the analytes are proteins. It acts as buffer, albeit a weak one, and generally the assumption is made that the buffer action is the cause for its popularity. But ammonium acetate has another most useful property. It leads to very clean mass spectra solely due to the protonated protein. As a result of the “salting-out” precipitation procedure used in the isolation of proteins, sodium ions are a very common impurity in protein samples. Use of ammonium acetate prevents the formation of sodium adducts to the protein. The results described in the preceding part (a) provide the mechanism by which this occurs. The ion-pairing reactions in the presence of ammonium acetate are shown in Eq. 1.20.



For simplicity, the equation shows only one ionized basic and acidic residue of the protein. The much larger concentration of the ammonium acetate relative to the sodium ion impurity

leads to ion pairing that involves only acetate and ammonium ions. Subjecting the resulting protein to collisional activation in the gas phase leads to facile loss of acetic acid and ammonia as shown in Eq. 1.21.



The dissociation is facile because the bond energy for the dissociation is only 15 kcal/mol for acetic acid and 11 kcal/mol for ammonia.<sup>58a</sup> The net effect of the complete process [Eqs. 1.20 and 1.21] is equivalent to a proton transfer from the ionized basic site to the ionized acidic site. Thus the molecular weight of the protein was not changed, but the positive and negative groups were neutralized. Thus a clean mass spectrum of the protein is obtained without a mass change.

Equations 1.20 and 1.21 show that any negative ion impurities due to anions of strong acids, such as the phosphate or trifluoroacetate anions, which would have led to strongly bonded adducts to the ionized basic residue [see Eq. 1.20], would also have been prevented by the relatively much higher concentration of the acetate ion from the ammonium acetate used. An important example is the use of trifluoroacetic acid mobile phase in liquid chromatography–mass spectrometry.<sup>58b</sup> The presence of the TFA anion in the effluent leads to a large loss of sensitivity in ESIMS and addition of ammonium acetate to the solution removes that loss.<sup>58b</sup>

### ***1.2.13.3 Determinations by Electrospray of Equilibrium Constants of Association Reactions in Solution and Possible Sources of Error Due to the ESI Process***

The determinations of equilibrium constants by ESIMS can be divided into two categories: (a) equilibria involving macro ions such as proteins and ligands which may be large organic molecules and (b) equilibria involving small reactant ions and ligands. Uncritical application of ESIMS can lead to erroneous results due to the complexity of the electrospray process. The determination of the association constants of protein–substrate complexes via NanoESI is well-developed and used, while that for small molecule complexes is not. Therefore, only the protein work will be considered here. Readers interested in small reactants equilibria can find useful literature information in the recent work by Zenobi and co-workers.<sup>59</sup> This work reports also new very interesting results based on measurements of laser-induced fluorescence and phase Doppler anemometry with which it was possible to measure the state of equilibrium inside individual charged and evaporating small droplets!

The formation of noncovalently bonded complexes of proteins with substrates is an extremely important class of reactions in biochemistry.<sup>41d</sup> It involves processes such as enzyme–substrate interactions, receptor–ligand binding, assembly of transcription complexes, and so on. The determination of these constants in solution has been an important component of biochemistry for many years. The established methods have various limitations, such as the requirement of large samples (X-ray crystallography), limited analyte molecular mass range (NMR), and poor mass resolution (gel electrophoresis). The major advantage of ESI is the very much smaller quantity of analyte required and the ability to identify also complexes involving multiple components. The first ESIMS study of non-covalent complexes involving proteins, by Ganem and Henion,<sup>60a</sup> was followed by a large number of studies which included quantitative determinations of the equilibrium constants.

References<sup>60b-63</sup> provide a sample of this work. Standing and co-workers<sup>60b</sup> demonstrated that reliable equilibrium constants for protein–substrate equilibria can be obtained with ESIMS.

Consider the general reaction [Eq. (22a)] where P is the protein and S is the substrate, and the reaction has reached equilibrium in the solution used. The equilibrium constant  $K_{AS}$  for the association reaction [Eq. (22a)] is given by Eq. (22b), where [P], [S], and [PS] are the concentrations at equilibrium.



$$K_{AS} = [PS]/[P] \times [S] = I_{PS}/I_P \times I_S \quad (1.22b)$$

Sampling the solution with ESI, the concentrations can be replaced with the ESIMS observed peak intensities,  $I_P$ ,  $I_S$ , and  $I_{PS}$ . It should be noted that the charges on P, S, and PS leading to the ions  $I_P$ ,  $I_S$ , and  $I_{PS}$  are, in general, not equal to the charge of these species in the solution, because multiple charges such as multiple  $H^+$  ions are supplied from the surface of the very small droplets leading to the gas-phase analytes by either ion evaporation IEM or the charged residue CRM model (see Sections 1.2.9 and 1.2.10).

One can repeat the experiment at several, gradually increasing concentrations of S and examine if the association constant, evaluated with Eq. (22b), remains constant. This procedure is called the “Titration Method.” ESIMS determinations of  $I_{PS}/I_P \times I_S$  with this method have been often in agreement with the requirements of Eq. (22b) and have also provided  $K_{AS}$  values in agreement with data in the literature obtained by conventional methods.<sup>60b-63</sup> When the molecular mass of S is much smaller than those of P and PS, as is often the case, erroneous results may be obtained due to  $m$  and  $m/z$  factors including the transmission of the MS analyzer. Therefore, it is advantageous to use only the ratio of  $I_{PS}/I_P$ , because P and PS have a similar mass when S is smaller than P, which is often the case. Zenobi and co-workers<sup>63</sup> have provided an equation for the determination of  $K_{AS}$  with the titration method in which  $I_S$  is eliminated.

From the standpoint of the mechanism of ESI, the agreement of the  $K_{AS}$  values determined via ESIMS with values obtained with other methods may appear surprising. One could expect that the very large increase of the concentration of the solutes in the charged droplets, due to evaporation of the solvent from the droplets, before the analytes are converted to gas-phase ions, will lead to an apparent  $K_{AS}$  that is much too high. However, this equilibrium shift need not occur if rates of the forward and reverse reactions leading to the equilibrium are slow compared to the time of droplet evaporation.

Peschke et al.,<sup>32</sup> using experimental information<sup>25a</sup> on the evaporation of charged water droplets produced by ESI and their fissions, evaluated an approximate droplet history scheme for water droplets produced by nanoelectrospray. The early part of this scheme is shown in Figure 1.6 (Section 1.2.7). Because the initial droplets produced by nanospray are very small ( $>1 \mu\text{m}$  in diameter), their evaporation is very fast so that they reach the Rayleigh instability condition in just several microseconds (see Figure 1.6). It could be established<sup>32</sup> that the first-generation progeny droplets will be the major source of analyte ions. Assuming even the fastest possible reaction rates (i.e., the diffusion limit rates) in water for the forward reaction  $P + S = PS$ , it could be shown that the time can be too short for the equilibrium [Eq. (22)] to shift in response to the increasing concentration due to solvent evaporation. The rate constant at the diffusion limit decreases with an increase of the substrate S size. Substrates of medium size such as erythrohydroxy aspartate, adenosine diphosphate, and adenosine triphosphate, with diffusion-limited rate constants from  $k = 10^6$ – $10^7 \text{ M}^{-1} \text{ s}^{-1}$ , are too slow to cause an equilibrium shift that will lead to a significant error in the

equilibrium constant ( $K_{AS}$ ) determination via ESIMS. Thus, an equilibrium shift for substrates that are not too small is not expected at least with nanospray.

The droplet evolution history<sup>32</sup> was based also on determinations by Gomez and Tang<sup>24</sup> which indicated that a small number of progeny droplets is emitted at each Rayleigh fission and that the diameters of the progeny are relatively large. The recent results by Duft et al.<sup>28b</sup> (see Table 1.2) predict a very much larger number of very much smaller progeny droplets. Because the smaller progeny droplets will evaporate much faster, one might expect that substrates S of considerably smaller size will also not lead to an equilibrium shift.

Because proteins are most probably transferred to the gas phase via CRM, another question must be examined also. Assuming that close to equal concentrations of the protein and substrate, in the 10  $\mu\text{M}$  range, were used, the evaluation<sup>32</sup> shows that in most cases there will be one protein and one substrate molecule in the average first-generation progeny droplet that has evaporated down to the size of the protein. In that case, the P and S will form a nonspecific complex because the substrate S makes a random encounter with the protein and has “no time” to find the site of specific strong bonding. Since the mass of the nonspecific complex is the same as that of the specific complex, the observed peak intensity,  $I_{SP}$ , will lead to an apparent  $K_{AS}$  that is too high. But this need not be the case. The weakly bonded nonspecific complexes are expected to fall apart easily in the clean-up stages of the interface to the mass analysis region, thereby minimizing the nonspecific contribution in the measured  $K_{AS}$ .<sup>32</sup>

The above *a priori* assumption about nonspecific complexes, while logical, may not predict the correct outcome in all cases. It neglects to consider the strong ion-neutral bonding in the gas phase discussed in Section 1.2.12 and Table 1.3 and the fact that the protein will be multiply charged as the charged droplet dries out. Strong hydrogen bonds can form between charged (protonated) sites of the protein and functional groups of the substrate such as -OH and -NH<sub>2</sub> groups. A recent study by Wang, Kitova, and Klassen<sup>65</sup> described exactly such effects for protein-carbohydrate protein-substrate complexes. Not only did they observe PS and SPS complexes in the gas phase, but the nonspecific bond was found to be stronger than the specific bond. This suggested that the nonspecific S-P bond was to a protonated site of the charged protein. The bond energies were determined with the Blackbody Infrared Radiative Dissociation (BIRD) technique with a modified Fourier Transfer Ion Cyclotron (FTICR) mass spectrometer.<sup>65</sup> Later work from this group<sup>66</sup> describes a method with which corrections can be made for the presence of nonspecific protein-substrate complexes.

### 1.2.14 Nanoelectrospray and Insights into Fundamentals of Electrospray–Nanospray

Nanospray was developed by Wilm and Mann,<sup>67,68</sup> whose primary interest was an electrospray with which much smaller quantities of analyte are required. Such a device would be particularly important to applications in biochemistry and particularly the analysis of proteins where, in general, very small samples are available. With ESI, most of the analyte is wasted. The large diameter of the spray tip produces large droplets whose evolution to small droplets requires the presence of a large distance between the spray tip and the sampling orifice (or sampling capillary) (see Figures 1.1 and 1.2a). As a result, only a very small fraction of the ultimate, very small droplets enters the sampling orifice (capillary). With nanospray, the spray tip has a much smaller diameter. Also, the flow is not a forced

flow, due to a driven syringe, as used in ESI (see Figure 1.2a); instead, the entrance end of the spray capillary is left open. A “self-flow” results, which is due to the pull of the applied electric field on the solution at the capillary tip (see Section II.B). The self-flow is controlled by the diameter of the tip of the spray capillary.

In their first effort,<sup>67</sup> using what was essentially an electrospray source, Wilm and Mann developed an equation for the radius of the zone at the tip of the Taylor cone from which the charged droplets are ejected. This radius is related to the resulting droplets' radii. It was found that the radius depends on the  $2/3$  power of the flow rate. To minimize the radius of the zone, a modified electrospray ion source with a smaller orifice was developed which led to a “microspray” version of ESI. Further development<sup>68</sup> using capillary orifices as small as 1–2  $\mu\text{m}$  in diameter led to nanospray. Such small orifices could be obtained<sup>68</sup> by pulling small-diameter borosilicate capillaries with a microcapillary puller. About 1  $\mu\text{L}$  of solvent is loaded directly into the entrance end of the capillary. The droplets produced past the capillary tip had a volume that was close to 1000 times smaller than the volume of droplets obtained with conventional ESI. Such small droplets will evaporate very rapidly, so that the capillary tip can be placed very close to the sampling orifice that leads to the mass spectrometer, thereby minimizing sample loss and allowing efficient use of a large fraction of the solution subjected to MS analysis. Thus, even though the amount of analyte sample is 10–100 times smaller than used with ESI, the observed mass spectrum peak intensities are equal to, if not better than, those in conventional ESI.

Another advantage of nanospray was the observation that with nanospray one can use neat water as a solvent without causing electric gas discharges as is the case with electrospray (see Section 1.2.4). Water as solvent is more suitable for the analysis of proteins, some of which may denature at least partially in other solvents.

Nanoelectrospray has proven to be of enormous importance to the analysis of biochemical and biopharmaceutical samples. However, it is also important to research on the fundamentals of electrospray—nanospray. Karas and co-workers<sup>69–71</sup> have been major contributors to this research. The experimental finding that mass spectra of analytes such as proteins obtained with nanospray are much less affected by the presence of impurities in the solution such as sodium compared to electrospray spectra is an advantage of nanospray. The reasons for this were examined<sup>69</sup> and the following reason was given. Gas-phase ions are produced from charged droplets only when the droplets are very small. This holds for both IEM and CRM. Therefore, if one starts with relatively small initial droplets, as is the case with nanospray, much less solvent evaporation will be required to reach the small size droplets required. Therefore, in the presence of impurities such as sodium salts the concentration increase of the salt will be much smaller with nanospray.

Mass spectra were obtained<sup>69</sup> with nanospray and electrospray. First, large concentrations ( $10^{-2}$  mol/L NaCl) in a solution of  $\text{H}_2\text{O}:\text{MeOH}:\text{HOAc}$  (48:48:4 vol%) and no protein were used. The nanospray spectra showed distinct peaks  $\text{Na}_n\text{Cl}_{n-1}^+$ , where  $n$  was between 9 and 32 and  $\text{Na}_n\text{Cl}_{n-2}^{2+}$  with roughly twice higher  $n$ . With electrospray the same peaks were observed, but also a forest of peaks spread over the whole mass range as would be expected from final droplets that had much higher solute concentrations. (*Note:* All mass spectra discussed were obtained in the  $m/z$  200–2000 range.)

More interesting were the spectra obtained with nanospray and electrospray and the solutes, insulin at  $10^{-5}$  mol/L and NaCl  $10^{-2}$  mol/L in the same  $\text{H}_2\text{O}:\text{MeOH}:\text{HOAc}$  solvent (see Figure 1.2b,c in Ref. <sup>69</sup>). The electrospray spectrum was dominated by a forest of closely spaced peaks due to Na and Cl containing clusters so that the protein could be barely found. With nanospray, the protein peaks were very clearly visible and in spite of the 1000 times larger concentration of NaCl, the combined peak intensity of the insulin ions was close

to equal, if not larger than, that of all the only Na- and Cl-containing ion clusters in the spectrum. This and other evidence made the authors consider that the charged insulin gas-phase ions are produced by a special process that leads to high peak intensity. Insulin is a rather small protein and can be considered also to be a peptide, but the implication of the discussion<sup>65</sup> is that the same process could be also valid for many, if not all, proteins.

It was proposed that the charged protein leaves the parent droplet. Thus, this is an IEM-type model but with special features. It was assumed that insulin is surface-active and therefore is present in enriched levels on the droplet surface. Some of the positively charged functional groups, such as protonated basic residues, reach the surface and become part of the charges at the surface of the droplet. If the basic residues were not protonated, they could become protonated by  $\text{H}_3\text{O}^+$  charges on the surface of the droplet.  $\text{Na}^+$  ions on the droplet surface can also form complexes with basic groups of the protein. Significantly, the basic sites on the surface of the protein will be closer together than the normal spacing of the charges on the droplet. The resulting uneven Coulomb repulsion between the charges on the droplet and the protein will force the protein charges outward, and this causes a bulge in the droplet (see Figure 1.5 in Ref. 65). The charged bulge will destabilize the droplet and lead to a droplet fission that expels the protein before the Rayleigh limit. This process may lead to an especially high yield of gas-phase protein ions.

The insulin spectra (see Figure 1.2b in Ref. 69) show groups of peaks for each charge state,  $Z = 3-5$ , with  $Z = 5$  being the dominant group of peaks. The major peak of each charge state is due to all charges being  $\text{H}^+$  ions. Peaks where one, two, and so on,  $\text{H}^+$  charges are replaced by  $\text{Na}^+$ , with gradually decreasing intensities, follow. The charging by  $\text{H}^+$  should in large part be due to the presence of HOAc in the solution. The pH was 2.5, which means a  $[\text{H}^+] \approx 3 \times 10^{-3}$  mol/L. This is close to the  $10^{-2}$  mol/L NaCl concentration used. Therefore, one can expect that the charges on the final droplets will not only be due to  $\text{Na}^+$  ions, but will also be due to  $\text{H}^+$  ions.

It was also observed<sup>65</sup> that the ratio of  $\text{Na}^+$  to  $\text{H}^+$  charges of the protein increases greatly with decreasing charge  $Z$  state of the protein (see Figure 1.2b in Ref. 69). The authors<sup>65</sup> explain this observation on the basis of the same model. They assume that the lower charge ions result from progeny droplets originating from parent droplets that had experienced many Coulomb fissions and, due to the solvent loss required for each fission, contain a large concentration of electrolyte. This large concentration increases the probability of negative ions such as  $\text{Cl}^-$  or  $\text{CH}_3\text{CO}_2^-$  to form ion pairs with ionized positively charged basic residues of the protein. These proteins then lose HCl or  $\text{CH}_3\text{CO}_2\text{H}$ , respectively, in the heated (200 °C) transfer capillary to the ion trap MS that was used. For evidence of such loss processes see Section 1.2.13 and Verkerk and Kebarle<sup>58a</sup>. The overall process reduces the charge of the observed protein ions. Due to the large  $\text{Na}^+ \text{X}^-$  concentration in these parent droplets, the protein ions will also have incorporated more Na impurities as observed in the mass spectrum (Figure 1.2b in Ref. 69). (*Note:* The above discussion of the model proposed by Karas and co-workers<sup>69</sup> differs somewhat from that given in Ref. 69. This was done in order to include information based on more recent work<sup>58a</sup>).

In an extension and expansion of the above work, Schmidt et al.<sup>70</sup> studied the effect of different solution flow rates on the analyte signal. A series of analytes was chosen: detergents, peptides, and oligosaccharides, which have decreasing surface activities. The authors found that the ion abundance of the analyte with low surface activity was suppressed at higher flow rates, while at the very lowest flow rates the suppression disappeared. The high flow rates were close to the regime for conventional ESI, whereas the lowest flow rate was in the low nano region. This result was rationalized as follows. At high flow rates,

the charged droplets emitted from the spray tip are much larger and the droplet history involving evaporation, droplet fission, progeny droplet evaporation, and fission until the very small final droplets are formed that lead to gas-phase ions is much longer. Surface-active analytes that will be enriched at the droplet surface will preferentially enter the progeny droplets and therefore will be enriched in the final generation progeny droplet, and this will lead to a high ion abundance for the surface active analyte. For the very small initial droplets obtained with lowest-flow nanospray, the evolution to the final droplet will be very short. In the extreme, there would be no such evolution, and this will lead to minimal discrimination against the non-surface-active analytes.

Another well-documented work by Chernushevich, Bahr, and Karas<sup>71</sup> deals with a disadvantage of nano relative to conventional electrospray. Using nanospray and repeated mass scans, some analytes were found to appear with delays of tens of minutes and a few were not detected at all, while no such suppression was found with ESI. The effect was found to be related to cation exchange chromatography on glass surfaces where the glass surface is negatively charged and retains positive ions. Peptides and proteins having a localization of positive charge where two or three ionized basic residues of the peptide or protein were in adjacent positions were most delayed or even completely suppressed. The very-small-diameter spray capillaries used in nano ESI lead to a high capillary surface-to-volume ratio and thus to a greatly increased exposure of negatively charged surface which delays or even traps the positive groups of the analytes. Replacing the glass with silica capillaries removed the analyte discrimination problem. Silica capillaries do not develop negative surfaces, whereas glass (sodium silicate) does. Presumably, with sodium silicate glass, some of the  $\text{Na}^+$  gets washed out, leaving behind negative silicate sites on the surface facing the solvent, whereas with fused silica no such process is possible.

## REFERENCES

- FENN, J. B. Electrospray wings for molecular elephants. Nobel Lecture available on web: [http://nobelprize.org/nobel\\_prizes/chemistry/laureates/2002/fenn-lecture.pdf](http://nobelprize.org/nobel_prizes/chemistry/laureates/2002/fenn-lecture.pdf)
- (a) CHAPMAN, S. Carrier mobility spectra of spray electrified liquids. *Phys. Rev.* **1937**, 52, 184–190.  
(b) CHAPMAN, S. Carrier mobility spectra of liquids electrified by bubbling. *Phys. Rev.* **1938**, 54, 520–527.  
(c) CHAPMAN, S. Interpretation of carrier mobility spectra of liquids electrified by bubbling and spraying. *Phys. Rev.* **1938**, 54, 528–533.
- DOLE, M. *My Life in the Golden Age of America*, Vantage Press, New York, **1989**, p. 169.
- DOLE, M.; MACK, L. L.; HINES, R. L.; MOBLEY, R. C.; FERGUSON, L. D.; ALICE, M. B. Molecular beams of macroions. *J. Chem. Phys.* **1968**, 49, 2240–2249.
- (a) YAMASHITA, M.; FENN, J. B. Electrospray ion source. Another variation of the free-jet theme. *J. Phys. Chem.* **1984**, 88, 4451–4459. (b) YAMASHITA, M.; FENN, J. B. Negative ion production with the electrospray ion source. *J. Phys. Chem.* **1984**, 88, 4672–4675.
- WHITEHOUSE, C. M.; DREYER, R. N.; YAMASHITA, M.; FENN, J. B. Electrospray interface for liquid chromatographs and mass spectrometers. *Anal. Chem.* **1985**, 57, 675–679.
- (a) SMITH, R. D.; LOO, J. L.; OGORZALEK LOO, R. R.; BUSMAN, M.; UDSETH, H. R. Principles and practice of electrospray ionization mass spectrometry for large peptides and proteins. *Mass Spectrom. Reviews* **1991**, 10, 359–451. (b) BAYLEY, A. G. *Electrostatic Spraying of Liquids*. John Wiley & Sons, New York, **1988**.  
(c) Electrospray: Theory and applications. Special issue of *J. Aerosol Sci.* **1994**, 25, 1005–1252.
- (a) LOEB, L.; KIP, A. F.; HUDSON, G. G.; BENNET, W. H. Pulses in negative point-to-plane corona. *Phys. Rev.* **1941**, 60, 714–722. (b) PFEIFER, R. J.; HENDRICKS, C. D. Parametric studies of electrohydrodynamic spraying. *AIAAJ* **1968**, 6, 496–502.
- TAYLOR, G. I. The stability of horizontal fluid interface in a vertical electric field. *J. Fluid. Mech.* **1965**, 2, 1–15.
- FERNANDEZ DE LA MORA, J. The fluid dynamics of Taylor cones. *J. Annu. Rev. Fluid. Mech.* **2007**, 39, 217–243.
- (a) CLOUPEAU, M.; PRUNET-FOCH, B. Electrohydrodynamic spraying functioning modes: A critical review. *J. Aerosol Sci.* **1994**, 25, 1021–1036. (b) CLOUPEAU, M. Recipes for use of EHD spraying in one-jet mode and notes on corona discharge. *J. Aerosol Sci.* **1994**, 25, 1143–1157. (c) CLOUPEAU, M.; PRUNET-FOCH, B. Recipes for use of EHD spraying of liquids in cone-jet mode. *J. Aerosol Sci.* **1989**, 22, 165–184. (d) MARGINEAN, I.;

- PARVIN, L.; HEFFERNAN, L.; VERTES, A. Flexing the electrified meniscus: The birth of a jet in electrosprays. *Anal. Chem.* **2004**, *76*, 4202–4207.
12. (a) TANG, K.; GOMEZ, A. On the structure of an electrospray of monodisperse droplets. *Phys. Fluids* **1994**, *6*, 2317–2322. (b) TANG, K.; GOMEZ, A. Generation by electrospray of monodisperse water droplets for targeted drug delivery by inhalation. *J. Aerosol Sci.* **1994**, *25*, 1237–1249. (c) TANG, K.; GOMEZ, A. Generation of monodisperse water droplets from electrosprays in a corona-assisted cone-jet mode. *J. Colloid Sci.* **1995**, *175*, 326–323. (d) TANG, K.; GOMEZ, A. Monodisperse electrosprays of low electric conductivity liquids in the cone-jet mode. *J. Colloid Sci.* **1996**, *184*, 500–511.
  13. BLADES, A. T.; IKONOMOU, M. G.; KEBARLE, P. Mechanism of electrospray mass spectrometry. Electrospray as an electrolysis cell. *Anal. Chem.* **1991**, *63*, 2109–2114.
  14. VAN BERKEL, G. J.; ZHOU, F.; ARONSON, J. T. Changes in bulk solution pH caused by the inherent controlled-current electrolytic process of an electrospray ion source. *Intern. J. Mass Spectrom. Ion Process.* **1997**, *162*, 55–62.
  15. FERNANDEZ DE LA MORA, J.; VAN BERKEL, G. J.; ENKE, C. G.; COLE, R. B.; MARTINEZ-SANCHEZ, M.; FENN, J. B. Electrochemical processes in electrospray ionization mass spectrometry. *J. Mass Spectrom.* **2000**, *35*, 939–952.
  16. SMITH, D. P. H. The electrohydrodynamic atomization of liquids. *IEEE Trans. Ind. Appl.* **1986**, *22*, 527–535.
  17. IKONOMOU, M. G.; BLADES, A. T.; KEBARLE, P. Electrospray mass spectrometry of methanol and water solutions. Suppression of electric discharge with SF<sub>6</sub> gas. *J. Am. Soc. Mass Spectrom.* **1991**, *2*, 497–505.
  18. WAMPLER, F. W.; BLADES, A. T.; KEBARLE, P. Negative ion electrospray mass spectrometry of nucleotides: Ionization from water solution with SF<sub>6</sub> discharge suppression. *J. Am. Soc. Mass Spectrom.* **1993**, *4*, 289–295.
  19. (a) FERNANDEZ DE LA MORA, J.; LOCERTALES, I. G. The current emitted by highly conducting Taylor cones. *J. Fluid. Mech.* **1994**, *260*, 155–184.
  20. CHERNEY, L. T. Structure of the Taylor cone jets: Limit of low flow rates. *J. Fluid. Mech.* **1999**, *378*, 167–196.
  21. CHEN, D. R.; PUI, D. Y. H. Experimental investigations of scaling laws for electrospray: Dielectric constant effect. *Aerosol Sci. Technology* **1997**, *27*, 367–380.
  22. LORD, Rayleigh; On the equilibrium of liquid conducting masses charged with electricity. *Philos. Mag. Ser. 5* **1882**, *14*, 184–186.
  23. DAVIS, E. J.; BRIDGES, M. A. The Rayleigh limit of charge revisited; light scattering from exploding droplets. *J. Aerosol Sci.* **1994**, *25*, 1179–1191.
  24. GOMEZ, A.; TANG, K. Charge and fission of droplets in electrostatic sprays. *Phys. Fluids* **1994**, *6*, 404–414.
  25. (a) SMITH, J. N.; FLAGAN, R. C.; BEAUCHAMP, J. L. Droplet evaporation and discharge dynamics in electrospray ionization. *J. Phys. Chem. A.* **2002**, *106*, 9957–9967. (b) GRIMM, R. L.; BEAUCHAMP, J. L. Evaporation and discharge dynamics of highly charged droplets of heptane, octane and *p*-xylene generated by electrospray ionization. *Anal. Chem.* **2002**, *74*, 6291–6297.
  26. TAFLIN, D. C.; WARD, T. L.; DAVIS, E. J. Electrified droplet fission and the Rayleigh limit. *Langmuir* **1989**, *5*, 376–384.
  27. RICHARDSON, C. B.; PIGG, A. L.; HIGHTOWER, R. L. On the stability limit of charged droplets. *Proc. Roy. Soc. A.* **1989**, 417–423.
  28. (a) SCHWEITZER, J. W.; HANSON, D. N. Stability limit of charged drops. *J. Colloid Interface Sci.* **1971**, *35*, 417–423. (b) DUFT, D.; ACHTZEHN, T.; MÜLLER, R.; HUBER, B. A.; LEISNER, T. Rayleigh jets from levitated microdroplets. *Nature* **2003**, *421*, 128–128.
  29. (a) LOCERTALES, I. G.; FERNANDEZ DE LA MORA, J. Experiments on the kinetics of field evaporation of small ions from droplets. *J. Chem. Phys.* **1995**, *103*, 5041–5060. (b) GAMERO-CASTANO, M.; FERNANDEZ DE LA MORA, J. Kinetics of small ion evaporation from the charge and mass distribution of multiply charged clusters in electrosprays. *J. Mass Spectrom.* **2000**, *35*, 790–803. (c) GAMERO-CASTANO, M.; FERNANDEZ DE LA MORA, J. Direct measurement of ion evaporation kinetics from electrified liquid surfaces. *J. Chem. Phys.* **2000**, *113*, 815–832.
  30. (a) GRIMM, R. L.; BEAUCHAMP, J. L. Dynamics of field induced droplet ionization: Time resolved studies of distortion, jetting and progeny formation from charged and neutral methanol droplets exposed to strong electric fields. *J. Chem. Phys. B* **2005**, *109*, 8244–8250. (b) GRIMM, R. L.; BEAUCHAMP, J. L. Field induced droplet ionization mass spectrometry. *J. Chem. Phys. B* **2003**, *107*, 14161–14163.
  31. HAGER, D. B.; DOVICH, N. J.; KLASSEN, J. S.; KEBARLE, P. Droplet electrospray mass spectrometry. *Anal. Chem.* **1994**, *66*, 3944–3949.
  32. PESCHKE, M.; VERKERK, U. H.; KEBARLE, P. Features of the ESI mechanism that affect the observation of multiply charged noncovalent complexes and the determination of the association constant by the titration method. *J. Am. Soc. Mass Spectrom.* **2004**, *15*, 1424–1434.
  33. SCHMELZEISEN-REDEKER, G.; BUTTERING, L.; ROLLGEN, F. W. Desolvation of ions and molecules in thermospray mass spectrometry. *Int. J. Mass Spectrom. Ion Proc.* **1989**, *90*, 139–150.
  34. (a) IRIBARNE, J. V.; THOMSON, B. A. On the evaporation of small ions from charged droplets. *J. Chem. Phys.* **1976**, *64*, 2287–2294. (b) THOMSON, B. A.; IRIBARNE, J. V. Field induced ion evaporation from liquid surfaces at atmospheric pressure. *J. Phys. Chem.* **1979**, *71*, 4451–4463.
  35. TANG, L.; KEBARLE, P. Dependence of the ion intensity in electrospray mass spectrometry on the concentration of the analytes in the electrosprayed solution. *Anal. Chem.* **1993**, *65*, 3654–3668.

36. (a) KEARLE, P.; PESCHKE, M. On the mechanism by which the charged droplets produced by electrospray lead to gas phase ions. *Analyt. Chim. Acta* **2000**, 406, 11–35. (b) KEARLE, P. A brief overview of the present status of the mechanisms involved in electrospray mass spectrometry. *J. Mass Spectrom.* **2000**, 35, 804–817. (c) COLE, R. B. Some tenets pertaining to electrospray ionization mass spectrometry. *J. Mass Spectrom.* **2000**, 35, 763–772.
37. (a) FENG, X.; BOGDAN, M. J.; AGNES, R. Coulomb fission event resolved progeny droplet production from isolated evaporating methanol droplets. *Anal. Chem.* **2001**, 73, 4499–4507. (b) ROMERO, S.; BOCANEGRA, R.; FERNANDEZ DE LA MORA, J. Source of heavy molecular ions based on Taylor cones of ionic liquids operating in the pure ion evaporation regime. *J. Appl. Physics* **2003**, 94, 3599–3605.
38. (a) NOHMI, T.; FENN, J. B. Electrospray mass spectrometry of polyethylene glycols with molecular weights up to five million. *J. Am. Chem. Soc.* **1992**, 114, 3241–3246. (b) NGUYEN, S.; FENN, J. B. Gas phase ions of solute species from charged droplets of solutions. *Proc. Nat. Acad. Sci.* **2007**, 104, 1111–1117. (c) ZNAMENSKIY, V.; MARGINEAN, I.; VERTES, A. Solvated ion evaporation from charged water nanodroplets. *J. Phys. Chem. A* **2003**, 107, 7406–7412. (d) WINGER, B. A.; LIGHT-WAHL, K. J.; OGORZALEC LOO, R. R.; UDSETH, H. R.; SMITH, R. D. Observations and implications of high mass-to-charge ratio ions from electrospray ionization mass spectrometry. *J. Am. Soc. Mass. Spectrom.* **1993**, 4, 536–545.
39. (a) TOLIC, R. P.; ANDERSON, G. A.; SMITH, R. D.; BROTHERS, H. M.; SPINDLER, R.; TOMALIA, D. A. Electrospray ionization Fourier transform ion cyclotron resonance mass spectrometric characterization of high molecular mass starburst (TM) dendrimers. *Int. J. Mass Spectrom. Ion Proc.* **1997**, 165, 405. (b) CHERNUSCHEVICH, I. V. In Ens, W.; Standing, K. G.; Chernushevich, I. V. (Eds.), *New Methods for the Study of Biomolecular Complexes*, Kluwer Academic Publishers, Dordrecht, **1998**, p. 101. (c) WANG, G.; COLE, R. B. Effect of solution ionic strength on analyte charge state distributions in positive and negative electrospray. *Anal. Chem.* **1994**, 66, 3702–3708.
40. FERNANDEZ DE LA MORA, J. Electrospray ionization of large multiply charged species proceeds via Dole's charged residue mechanism. *Anal. Chim. Acta* **2000**, 406, 93–104.
41. (a) VALENTINE, S. J.; ANDERSON, J. G.; ELLINGTON, D. E.; CLEMMER, D. E. Disulfide intact and reduced lysozyme in the gas phase: Conformations and pathways of folding and unfolding. *J. Phys. Chem B* **1997**, 101, 3891–3900. (b) HUDGINS, R. R. High resolution ion mobility measurements for gas phase conformations. *Int. J. Mass Spectrom.* **1997**, 165, 497–507. (c) SHELIMOV, K. B.; CLEMMER, D. E.; HUDGINS, R. R.; JARROLD, M. Protein structure *in vacuo*: Gas phase conformations of BPTI and cytochrome C. *J. Am. Chem. Soc.* **1997**, 119, 2240–2248. (d) HECK, A. J. R.; van der HEUVEL, R. H. H. Investigation of intact protein complexes by mass spectrometry. *Mass Spectrom. Rev.* **2004**, 23, 368–389.
42. (a) SAMALIKOVA, M.; GRANDORI, R. Protein charge state distributions in electrospray ionization mass spectrometry do not appear to be limited by the surface tension of the solvent. *J. Am. Chem. Soc.* **2003**, 125, 13362–13365. (b) SAMALIKOVA, M.; GRANDORI, R. Testing the role of surface tension in protein ionization by mass spectrometry. *J. Mass Spectrom.* **2005**, 40, 503–510.
43. IAVARONE, A. T.; WILLIAMS, E. R. Mechanism of charging and supercharging molecules in electrospray. *J. Am. Chem. Soc.* **2003**, 125, 2319–2327.
44. IAVARONE, A. T.; WILLIAMS, E. R. Private communications to the authors.
45. VICAR, S.; MULKERIN, M. G.; BATHORY, G.; KHUNDKAR, L. H.; KARGER, B. L. Conformational changes in the reversed phase liquid chromatography of recombinant human growth hormone as a function of organic solvent: The molten globule state. *Anal. Chem.* **1994**, 66, 3908–3915.
46. KALTASHOV, I. A.; MOHIMEN, A. Estimates of protein areas in solution by electrospray ionization mass spectrometry. *Anal. Chem.* **2005**, 77, 5370–5379.
47. BENESCH, J. L. P.; ROBINSON, C. V. Mass spectrometry of macromolecular assemblies: Preservation and dissociation. *Current Opin. Struct. Biol.* **2006**, 16, 245–251.
48. ENKE, C. G. A predictive model for matrix and analyte effects in the electrospray ionization of singly-charged ionic analytes. *Anal. Chem.* **1997**, 69, 4885–4893.
49. NIST Database, <http://webbook.nist.gov>.
50. KAUZMANN, W. Some factors in the interpretation of protein denaturation. *Adv. Protein Chem.* **1959**, 14, 1–63.
51. DAVIDSON, W. R.; KEARLE, P. Binding energies and stabilities of potassium ion complexes from studies of the gas phase ion equilibria:  $K^+ + M = K^+ M$ . *J. Am. Chem. Soc.* **1979**, 98, 6133–6138.
52. SUNNER, J.; KEARLE, P. Ion-solvent molecule interactions in the gas phase. The potassium ion and Me<sub>2</sub>SO, DMA, DMF, and acetone. *J. Am. Chem. Soc.* **1984**, 106, 6135–6139.
53. (a) HOYAU, S.; NORRMAN, K.; MCMAHON, T. B.; OHANESSIAN, G. A. Quantitative basis scale of Na<sup>+</sup> affinities of organic and small biological molecules in the gas phase. *J. Am. Chem. Soc.* **1999**, 121, 8864–887. (b) MCMAHON, T. B.; OHANESSIAN, G. An experimental and *ab initio* study of the nature and binding of gas phase complexes of sodium ions. *Chem. Eur. J.* **2000**, 6, 2931–2935.
54. KLASSEN, J. S.; ANDERSON, S. G.; BLADES, A. T.; KEARLE, P. Reaction enthalpies for  $M + L = M + L$ , where  $M = Na^+, K^+$  and  $L =$  acetamide, *N*-methyl acetamide, *N,N*-dimethylacetamide, glycine, glycylglycine, from determinations of the

- collision-induced thresholds. *J. Phys. Chem.* **1996**, 100, 14218–14227.
55. (a) ARMENTROUT, P. B.; RODGERS, M. T. An absolute sodium cation affinity scale: Threshold Collision induced dissociation energies and *ab initio* theory. *J. Phys. Chem. A* **2000**, 104, 2238–2244.  
(b) AMICANGELO, J. C.; ARMENTROUT, P. B. Relative and absolute bond dissociation energies of sodium cation complexes determined using competitive collision-induced dissociation experiments. *Int. J. Mass Spectrom.* **2001**, 212, 301–325.
  56. (a) SU, T.; BOWERS, M. T. Ion–polar molecule collisions: The effect of ion size on ion–polar molecule rate constants; the parametrization of the average-dipole-orientation theory. *Int. J. Mass Spectrom. Ion Phys.* **1973**, 12, 347. (b) TALROSE, V. L.; VINOGRADOV, P. S.; LARIN, I. K. On the rapidity of Ion–molecule Reactions. In *Gas Phase Ion Chemistry*, Vol. 1, Bowers, M. T. (Ed.), Academic Press, New York, **1979**, Chapter 8.
  57. REINHOLD, V. N.; REINHOLD, B. B.; CASTELLO, C. E. Carbohydrate molecular weight profiling, sequence, linkage and branching data. *Anal. Chem.* **1995**, 67, 1772–1784.
  58. (a) VERKERK, U. H.; KEBARLE, P. Ion–ion and ion–molecule reactions at the surface of proteins produced by nanospray. Information on the number of acidic residues and control of the number of ionized acidic and basic residues. *J. Am. Soc. Mass Spectrom.* **2005**, 16, 1325–1341. (b) SHOU, W. Z.; NAIDONG, W. Simple means to alleviate sensitivity loss by trifluoroacetic acid (TFA) mobile phases in the hydrophilic interaction chromatography–electrospray tandem mass spectrometric bioanalysis of basic compounds. *J. Chromatogr. B* **2005**, 825, 186–192.
  59. WORTMAN, A.; KISTLER-MOMOTOVA, A.; ZENOBI, R.; HEINE, M. C.; WILHELM, D.; PRATSINIS, S. E. Shrinking droplets in electrospray ionization and their influence on chemical equilibria. *J. Am. Soc. Mass Spectrom.* **2007**, 18, 385–393.
  60. (a) GANEM, B.; LI, Y.; HENION, J. D. Detection of non-covalent acceptor–ligand complexes by mass spectrometry. *J. Am. Chem. Soc.* **1991**, 113, 6294–6296. (b) AYED, A.; KRUTCHINSKY, A. N.; ENS, W.; STANDING, K. G.; DUCKWORTH, H. W. Qualitative evaluation of protein–protein and ligand–protein equilibria of a large allosteric enzyme by electrospray ionization time of flight mass spectrometry. *Rapid Commun. Mass Spectrom.* **1998**, 12, 339–344.
  61. LOO, J. Studying noncovalent protein complexes by electrospray ionization mass spectrometry. *Mass Spectrom. Rev.* **1997**, 16, 1–23.
  62. DANIEL, J. M.; FRIESS, S. D.; RAJAGOPALAN, S.; WEND, S.; ZENOBI, R. Quantitative determination of noncovalent binding interactions using soft ionization mass spectrometry. *Int. J. Mass Spectrom.* **2002**, 216, 1–27.
  63. DANIEL, J. M.; MCCOMBIE, G.; WEND, S.; ZENOBI, R. Mass spectrometric determination of association constants of adenylate kinase with two noncovalent inhibitors. *J. Am. Soc. Mass Spectrom.* **2003**, 14, 442–448.
  64. PESCHKE, M.; VERKERK, U. H.; KEBARLE, P. Features of the ESI mechanism that affect the observation of multiply charged noncovalent complexes and the determination of the association constant by the titration method. *J. Am. Soc. Mass Spectrom.* **2004**, 15, 1424–1434.
  65. WANG, W.; KITOVA, E. N.; KLASSEN, J. S. Bioactive recognition sites may not be energetically preferred in protein–carbohydrate complexes in the gas phase. *J. Am. Chem. Soc.* **2003**, 125, 13630–13861.
  66. SUN, J.; KITOVA, E. N.; WANG, W.; KLASSEN, J. S. Method for distinguishing specific from nonspecific protein–ligand complexes in nanoelectrospray ionization mass spectrometry. *Anal. Chem.* **2006**, 78, 3010–3018.
  67. WILM, M.; MANN, M.; ELECTROSPRAY Taylor–Cone theory, Dole’s beam of macromolecules at last?. *Int. J. Mass Spectrom. Ion Proc.* **1994**, 136, 167–180.
  68. WILM, M.; MANN, M. Analytical properties of the nanoelectrospray ion source. *Anal. Chem.* **1996**, 68, 1–8.
  69. JURASHEK, R.; DULKS, T.; KARAS, M. Nanoelectrospray—More than just a minimized-flow electrospray ion source. *J. Am. Soc. Mass Spectrom.* **1999**, 10, 300–308.
  70. SCHMIDT, A.; KARAS, M.; DULKS, T. Effect of different solution flow rates on analyte signals in nano-ESI-MS, or when does ESI Turn into nano-ESI. *J. Am. Soc. Mass Spectrom.* **2003**, 14, 492–500.
  71. CHERNUSHEVICH, I. V.; BAHR, U.; KARAS, M. Nanospray taxation and how to avoid it. *Rapid Commun. Mass Spectrom.* **2004**, 18, 2479–2485.